though their unique functions have yet to be characterized (35). These TTP-related proteins are rapidly expressed in response to 12-*O*-tetradecanoylphorbol-13-acetate and other diverse stimuli in various types of eukaryotic cells (23,36). The expression of these proteins differs depending on the circumstances, hence they may have their own roles in controlling mRNA turnover under different circumstances (37). Among these proteins, TTP is induced by TNFα, suggesting that TTP may function as a feedback regulator of TNFα gene expression (31,38). Notably, a TIS11B homolog expressed rapidly in response to butyrate has also been discovered in human cells and characterized as butyrate response factor 1 (BRF1) (39).

Consistently, butyrate rapidly induced the expression of TIS11B in RAW264.7 cells (Figure 4A). In addition, the induction of TNFα mRNA by LPS stimulation was strongly inhibited when TIS11B was overexpressed in these cells (Figure 4B). Stoecklin et al identified BRF1 as a regulator of ARE-dependent mRNA decay, and also showed that BRF1 can bind directly to ARE and promote the degradation of ARE-containing mRNA (40). Thus, we postulated a model whereby butyrate induced the expression of TIS11B/BRF1, followed by the binding of this ARE-binding protein to the ARE, thus facilitating TNFα mRNA degradation. Our cDNA microarray (GeneNavigator cDNA Array System; Toyobo) revealed that butyrate suppressed expression of mRNA containing AREs in their 3′-UTRs (e.g., mRNA for IL-1β, IL-15, and granulocyte–macrophage colony-stimulating factor) (data not shown). This result further supported the relevance of our hypothesis.

TIS11B has a unique character that facilitates TNFα mRNA degradation; therefore, analyzing the regulation of this molecule would provide a novel approach to the control of TNFα production. TNFα expression is activated mainly by the transcription factor NF-κB and by the MAP kinase (MAPK) pathways (the ERK, JNK, and p38 MAPK pathways). Recent studies have shown that the p38 MAPK pathway in particular plays an important role in posttranscriptional regulation that leads to mRNA stabilization (41). The p38 MAPK pathway also strongly induces and activates TTP, which down-regulates TNFα (42–45). Those studies suggested that the p38 MAPK pathway may play a crucial role in regulating the expression of TNFα (involving a TTP-dependent mechanism); however, the precise mechanism is not completely understood, and less is known about the relationship between TIS11B and the p38 MAPK pathway. Since butyrate induced TIS11B expression and has been shown to affect the p38 MAPK pathway (46), it may be that butyrate influences TIS11B expression through the p38 MAPK pathway. Analysis of the relationship between TIS11B and the p38 MAPK pathway would be important for understanding the effect of butyrate.

The effects of butyrate on TNFα gene expression, other than those involving TIS11B- and ARE-dependent mechanisms, also need to be addressed. In previous studies, it was shown that butyrate can inhibit the binding of NF-κB to DNA (12,15,47). In contrast, in the reporter gene assays, butyrate enhanced the transcriptional activity driven by NF-κB sites and the TNFα promoter in a dose-dependent manner (Figures 3A and B). This phenomenon may be explained in part by the HDA-inhibitory effects of butyrate. Butyrate strongly inhibits HDA activity in cells, and it can cause hyperacetylation of nucleotides and thereby nonspecifically enhance transcriptional activity (18,48,49). As in the case of genomic DNA, transfected plasmid DNA has been shown to be assembled with histones to form a "minichromosome" that is sensitive to histone hyperacetylation (50). Thus, butyrate can function as a nonspecific transcriptional enhancer for transfected plasmid DNA; hence, cotransfection with an internal control was not informative in the current experiments.

Analysis of the regulation of TNFα by butyrate provides information for a novel approach to the treatment of patients with RA. Further investigation of the regulation of TIS11B expression, including study of its gene promoter, promises to pave the way for therapeutic approaches that address ARE-dependent cytokine gene regulation.

ACKNOWLEDGMENTS

We thank Ms Akiko Hirano and Ms Miki Aoto for technical assistance.

REFERENCES

1. Feldmann M, Brennan FM, Maini RN. Rheumatoid arthritis. Cell 1996;85:307–10.
2. Daniel CL, Moreland LW. Infliximab: additional safety data from an open label study. J Rheumatol 2002;29:647–9.
3. MacNaul KL, Chartrain N, Lark M, Tocci MJ, Hutchinson NI. Discoordinate expression of stromelysin, collagenase, and tissue inhibitor of metalloproteinases-1 in rheumatoid human synovial fibroblasts: synergistic effects of interleukin-1 and tumor necrosis factor-α on stromelysin expression. J Biol Chem 1990;265: 17238–45.
4. Chin JE, Winterrowd GE, Krzesicki RF, Sanders ME. Role of cytokines in inflammatory synovitis: the coordinate regulation of

intercellular adhesion molecule 1 and HLA class I and class II antigens in rheumatoid synovial fibroblasts. Arthritis Rheum 1990;33:1776–86.
5. Feldmann M, Brennan FM, Chantry D, Haworth C, Turner M, Abney E, et al. Cytokine production in the rheumatoid joint: implications for treatment. Ann Rheum Dis 1990;49:480–6.
6. Chu CQ, Field M, Feldmann M, Maini RN. Localization of tumor necrosis factor α in synovial tissues and at the cartilage–pannus junction in patients with rheumatoid arthritis. Arthritis Rheum 1991;34:1125–32.
7. Tak PP, Bresnihan B. The pathogenesis and prevention of joint damage in rheumatoid arthritis: advances from synovial biopsy and tissue analysis [review]. Arthritis Rheum 2000;43:2619–33.
8. Takayanagi H, Oda H, Yamamoto S, Kawaguchi H, Tanaka S, Nishikawa T, et al. A new mechanism of bone destruction in rheumatoid arthritis: synovial fibroblasts induce osteoclastogenesis. Biochem Biophys Res Commun 1997;240:279–86.
9. Zhang G, Ghosh S. Molecular mechanisms of NF-κB activation induced by bacterial lipopolysaccharide through Toll-like receptors. J Endotoxin Res 2000;6:453–7.
10. Choe JY, Crain B, Wu SR, Corr M. Interleukin 1 receptor dependence of serum transferred arthritis can be circumvented by toll-like receptor 4 signaling. J Exp Med 2003;197:537–42.
11. Bamba T, Kanauchi O, Andoh A, Fujiyama Y. A new prebiotic from germinated barley for nutraceutical treatment of ulcerative colitis. J Gastroenterol Hepatol 2002;17:818–24.
12. Inan MS, Rasoulpour RJ, Yin L, Hubbard AK, Rosenberg DW, Giardina C. The luminal short-chain fatty acid butyrate modulates NF-κB activity in a human colonic epithelial cell line. Gastroenterology 2000;118:724–34.
13. Weaver GA, Krause JA, Miller TL, Wolin MJ. Short chain fatty acid distributions of enema samples from a sigmoidoscopy population: an association of high acetate and low butyrate ratios with adenomatous polyps and colon cancer. Gut 1988;29:1539–43.
14. Kashtan H, Stern HS, Jenkins DJ, Jenkins AL, Thompson LU, Hay K, et al. Colonic fermentation and markers of colorectal-cancer risk. Am J Clin Nutr 1992;55:723–8.
15. Segain JP, Raingeard de la Bletiere D, Bourreille A, Leray V, Gervois N, Rosales C, et al. Butyrate inhibits inflammatory responses through NFκB inhibition: implications for Crohn's disease. Gut 2000;47:397–403.
16. Ahmad MS, Krishnan S, Ramakrishna BS, Mathan M, Pulimood AB, Murthy SN. Butyrate and glucose metabolism by colonocytes in experimental colitis in mice. Gut 2000;46:493–9.
17. Pazin MJ, Kadonaga JT. What's up and down with histone deacetylation and transcription? Cell 1997;89:325–8.
18. Espinos E, Le V, Thai A, Pomies C, Weber MJ. Cooperation between phosphorylation and acetylation processes in transcriptional control. Mol Cell Biol 1999;19:3474–84.
19. Atsumi T, Nishihira J, Makita Z, Koike T. Enhancement of oxidised low-density lipoprotein uptake by macrophages in response to macrophage migration inhibitory factor. Cytokine 2000; 12:1553–6.
20. Heid CA, Stevens J, Livak KJ, Williams PM. Real time quantitative PCR. Genome Res 1996;6:986–94.
21. Chen J, Amasaki Y, Kamogawa Y, Nagoya M, Arai N, Arai K, et al. Role of NFATx (NFAT4/NFATc3) in expression of immunoregulatory genes in murine peripheral CD4+ T cells. J Immunol 2003;170:3109–17.
22. Semon D, Kawashima E, Jongeneel CV, Shakhov AN, Nedospasov SA. Nucleotide sequence of the murine TNF locus, including the TNF-α (tumor necrosis factor) and TNF-β (lymphotoxin) genes. Nucleic Acids Res 1987;15:9083–4.
23. Ino T, Yasui H, Hirano M, Kurosawa Y. Identification of a member of the TIS11 early response gene family at the insertion point of a DNA fragment containing a gene for the T-cell receptor β chain in an acute T-cell leukemia. Oncogene 1995;11:2705–10.
24. Amasaki Y, Adachi S, Ishida Y, Iwata M, Arai N, Arai K, et al. A constitutively nuclear form of NFATx shows efficient transactivation activity and induces differentiation of CD4(+)CD8(+) T cells. J Biol Chem 2002;277:25640–8.
25. Van den Berg WB, van Lent PL. The role of macrophages in chronic arthritis. Immunobiology 1996;195:614–23.
26. McCarthy JE, Kollmus H. Cytoplasmic mRNA-protein interactions in eukaryotic gene expression. Trends Biochem Sci 1995;20: 191–7.
27. Xu N, Chen CY, Shyu AB. Modulation of the fate of cytoplasmic mRNA by AU-rich elements: key sequence features controlling mRNA deadenylation and decay. Mol Cell Biol 1997;17:4611–21.
28. Peng SS, Chen CY, Shyu AB. Functional characterization of a non-AUUUA AU-rich element from the c-jun proto-oncogene mRNA: evidence for a novel class of AU-rich elements. Mol Cell Biol 1996;16:1490–9.
29. Bakheet T, Frevel M, Williams BR, Greer W, Khabar KS. ARED: human AU-rich element-containing mRNA database reveals an unexpectedly diverse functional repertoire of encoded proteins. Nucleic Acids Res 2001;29:246–54.
30. Bakheet T, Williams BR, Khabar KS. ARED 2.0: an update of AU-rich element mRNA database. Nucleic Acids Res 2003;31: 421–3.
31. Carballo E, Lai WS, Blackshear PJ. Feedback inhibition of macrophage tumor necrosis factor-α production by tristetraprolin. Science 1998;281:1001–5.
32. Taylor GA, Carballo E, Lee DM, Lai WS, Thompson MJ, Patel DD, et al. A pathogenetic role for TNFα in the syndrome of cachexia, arthritis, and autoimmunity resulting from tristetraprolin (TTP) deficiency. Immunity 1996;4:445–54.
33. Carballo E, Gilkeson GS, Blackshear PJ. Bone marrow transplantation reproduces the tristetraprolin-deficiency syndrome in recombination activating gene-2 (−/−) mice: evidence that monocyte/macrophage progenitors may be responsible for TNFα overproduction. J Clin Invest 1997;100:986–95.
34. Phillips K, Kedersha N, Shen L, Blackshear PJ, Anderson P. Arthritis suppressor genes TIA-1 and TTP dampen the expression of tumor necrosis factor α, cyclooxygenase 2, and inflammatory arthritis. Proc Natl Acad Sci U S A 2004;101:2011–6.
35. Johnson BA, Geha M, Blackwell TK. Similar but distinct effects of the tristetraprolin/TIS11 immediate-early proteins on cell survival. Oncogene 2000;19:1657–64.
36. Varnum BC, Ma QF, Chi TH, Fletcher B, Herschman HR. The TIS11 primary response gene is a member of a gene family that encodes proteins with a highly conserved sequence containing an unusual Cys-His repeat. Mol Cell Biol 1991;11:1754–8.
37. Blackshear PJ. Tristetraprolin and other CCCH tandem zinc-finger proteins in the regulation of mRNA turnover. Biochem Soc Trans 2002;30:945–52.
38. Lai WS, Carballo E, Strum JR, Kennington EA, Phillips RS, Blackshear PJ. Evidence that tristetraprolin binds to AU-rich elements and promotes the deadenylation and destabilization of tumor necrosis factor α mRNA. Mol Cell Biol 1999;19: 4311–23.
39. Maclean KN, McKay IA, Bustin SA. Differential effects of sodium butyrate on the transcription of the human TIS11 family of early-response genes in colorectal cancer cells. Br J Biomed Sci 1998;55:184–91.
40. Stoecklin G, Colombi M, Raineri I, Leuenberger S, Mallaun M, Schmidlin M, et al. Functional cloning of BRF1, a regulator of ARE-dependent mRNA turnover. EMBO J 2002;21:4709–18.
41. Wang SW, Pawlowski J, Wathen ST, Kinney SD, Lichenstein HS, Manthey CL. Cytokine mRNA decay is accelerated by an inhibitor of p38-mitogen-activated protein kinase. Inflamm Res 1999;48:533–8.
42. Dean JL, Sully G, Clark AR, Saklatvala J. The involvement of AU-rich element-binding proteins in p38 mitogen-activated pro-

tein kinase pathway-mediated mRNA stabilisation. Cell Signal 2004;16:1113–21.
43. Mahtani KR, Brook M, Dean JL, Sully G, Saklatvala J, Clark AR. Mitogen-activated protein kinase p38 controls the expression and posttranslational modification of tristetraprolin, a regulator of tumor necrosis factor α mRNA stability. Mol Cell Biol 2001;21: 6461–9.
44. Tchen CR, Brook M, Saklatvala J, Clark AR. The stability of tristetraprolin mRNA is regulated by mitogen-activated protein kinase p38 and by tristetraprolin itself. J Biol Chem 2004;279: 32393–400.
45. Brooks SA, Connolly JE, Rigby WF. The role of mRNA turnover in the regulation of tristetraprolin expression: evidence for an extracellular signal-regulated kinase-specific, AU-rich element-dependent, autoregulatory pathway. J Immunol 2004;172:7263–71.
46. Daniel C, Schroder O, Zahn N, Gaschott T, Stein J. p38 MAPK signaling pathway is involved in butyrate-induced vitamin D receptor expression. Biochem Biophys Res Commun 2004;324: 1220–6.
47. Venkatraman A, Ramakrishna BS, Shaji RV, Kumar NS, Pulimood A, Patra S. Amelioration of dextran sulfate colitis by butyrate: role of heat shock protein 70 and NF-κB. Am J Physiol Gastrointest Liver Physiol 2003;285:G177–84.
48. Boffa LC, Vidali G, Mann RS, Allfrey VG. Suppression of histone deacetylation in vivo and in vitro by sodium butyrate: reversible effects of Na-butyrate on histone acetylation. J Biol Chem 1978; 253:3364–6.
49. Vidali G, Boffa LC, Mann RS, Allfrey VG. Reversible effects of Na-butyrate on histone acetylation. Biochem Biophys Res Commun 1978;82:223–7.
50. Reeves R, Gorman CM, Howard B. Minichromosome assembly of non-integrated plasmid DNA transfected into mammalian cells. Nucleic Acids Res 1985;13:3599–615.

Lupus (2005) 14, 799-801
www.lupus-journal.com

EDITORIAL

Antiphospholipid antibodies and cell activation: crucial role of p38 MAPK pathway

Antiphospholipid antibodies (aPL) are a large and heterogeneous family of circulating immunoglobulins found in a wide range of infectious and autoimmune diseases. Since the early 1980s, the interest on these antibodies has increased exponentially due to their associations with thrombotic events and pregnancy morbidity in the antiphospholipid syndrome (APS).[1]

Intensive research works, performed in the last decade, have greatly advanced our knowledge of the mechanisms that explain why these antibodies may play a direct role in clot formation. Nowadays, it is recognized worldwide that many of the autoantibodies associated with the APS are directed against phospholipid-binding plasma proteins such as β2-glycoprotein I (β2GPI) and prothrombin or phospholipid-protein complexes, expressed on, or bound to, the surface of vascular endothelial cells, platelets or other cells.[2]

One of the key events to explain the pathophysiology of thrombosis in patients with APS is the pro-coagulant cell activation mediated by aPL, accompanied with tissue factor (TF) expression and TF pathway up-regulation. TF is the major initiator of the extrinsic coagulation system, functioning in coagulation by serving as the protein cofactor for the activated factor VII (FVIIa).[3] Induced TF forms a complex with FVIIa that triggers blood clotting cascade by activating factors IX and X, leading to thrombin generation. In normal conditions, TF is not expressed on intravascular cells but it can be induced under some stimuli such as lipopolysaccharide, tumour necrosis factor α (TNFα), interleukin-1 (IL-1) and shear stress.[4]

Experimental data showed that plasma of patients with APS or purified aPL can activate endothelial cells or monocytes leading to the expression of adhesion molecules, TF and other pro-coagulant substances.[5] Furthermore, upregulation of TF in patients with APS has been demonstrated,[6,7] and we reported that antibodies against β2GPI induce the expression and activity of TF *in vitro*.[8] In addition, the binding of aPL to platelets, once stimulated, causes activation and aggregation of platelets and thrombosis.[9-14] Overall, the effect of aPL in pro-coagulant cell activation has been evident and recent research works have focused on the intracellular events involved in the aPL-mediated cell activation, trying to clarify the signal transduction mechanism implicated in the induction of pro-coagulants substances by aPL. As a result of these investigations, two groups independently reported that adaptor molecule myeloid differentiation protein (MyD88)-dependent signalling pathway is involved in endothelial cell activation by aPL.[15,16]

Several groups demonstrated the involvement of nuclear factor kappa B (NFkB) in endothelial cell activation.[17-19] IgG purified from APS patients induced the nuclear translocation of NFkB leading to the transcription of genes with NFkB-responsive element in their promoter. This nuclear translocation of NFkB, at least in part, mediates the increased expression of TF and adhesion molecules on cell surface.[18] NFkB blocking by statins inhibited endothelial cell activation mediated by anti-β2GPI antibodies and provide an additional use of statins as a therapeutic tool for the treatment of APS.[17]

Anti-β2GPI antibodies activate endothelial cell in a β2GPI-dependent manner, and this cell activation might require an interaction between β2GPI and a specific endothelial cell receptor. It has been shown that annexin II, an endothelial cell receptor for tissue plasminogen activator and plasminogen, behaved as a receptor for β2GPI.[20] However it is still unclear whether such a putative receptor is actually involved in cell activation because annexin II does not span the cell membrane and the presence of an unknown 'adaptor' was suggested to be necessary to induce activation. Raschi *et al.*[15] suggested a possible association between β2GPI and members of the Toll-like receptors (TLRs) family. They speculated that anti-β2GPI antibodies might cross-link β2GPI molecules likely together with TLRs, eventually favouring the receptor polymerization and the signalling cascade activation. Furthermore, Lutters *et al.*[21] showed that dimeric β2GPI can interact with apolipoprotein E receptor 2 (apoER2), a member of the low density lipoprotein receptor family present in platelets and that dimeric β2GPI induces increased platelet adhesion and thrombus formation, which depend on the activation of apoER2.

The p38 mitogen activated protein kinase (MAPK) pathway of cell activation has become an important focus of interest and it has been implicated in the

10.1191/0961203305lu2160ed

regulation of TF expression in monocytes and endothelial cells.[22–25] p38 MAPK pathway is a member of the protein kinase family, key regulators of cellular signalling that control inflammatory response, cell differentiation and cell growth, and can be activated by many stimuli including lipopolysaccharide, other bacterial products, cytokines or stress.[26] Activation of p38 MAPK pathway increases activities of inflammatory cytokines such as TNFα and IL-1β and is considered to be critical for normal immune responses.[27]

Last year, two independent groups demonstrated the crucial role of p38 MAPK in aPL-mediated cell activation.[28,29] Vega-Ostertag *et al.*[28] reported that phosphorylation of p38 MAPK is involved in aPL-mediated production of thromboxane by platelets. Pretreatment of platelets with SB203580, a p38 MAPK specific inhibitor, completely abrogated aPL-mediated platelet aggregation. Our group[29] showed that monocytes stimulation by monoclonal anti-β2GPI antibodies derived from APS patients induce phosphorylation of p38MAPK, locational shift of NFkB into the nucleus and up-regulation of TF expression. The TF expression occurs only in the presence of β2GPI, suggesting that perturbation of monocyte by anti-β2GPI antibodies is initiated by interaction between the cell and the autoantibody-bound β2GPI. Further, the involvement of p38MAPK activation on endothelial cells has been reported to be required in aPL-mediated prothrombotic status.[30]

The recognition of the crucial role of p38 MAPK in the intracellular activation mediated by aPL is a novel finding that represents a great advance in the understanding of the mechanisms involved in the production of the hypercoagulable state in patients with APS. Those researches may open new insights in the therapeutic approach of patients with APS and give a clue to establish a more specific target therapy by down-regulating the specific pathway of signal transduction.

Further studies are needed to clarify how aPL-phospholipid-binding complexes affect to cell surface molecule and how signal transduction events occur upstream of p38 MAPK.

References

1 Khamashta MA. Hughes syndrome: history. In: Khamashta MA, ed. *Hughes Syndrome: Antiphospholipid syndrome*. London: Springer-Verlag, 2000: 3–7.
2 Atsumi T, Matsuura E, Koike T. Immunology of antiphospholipid antibodies and co-factors. In: Lahita RG, ed. *Systemic lupus erythematosus*. San Diego: Academic Press, 2004: 1081–1105.
3 Mann K. Biochemistry and physiology of blood coagulation. *Thromb Haemost* 1999; **82**: 165–174.
4 Mackman N. Regulation of the tissue factor gene. *Faseb J* 1995; **9**: 883–889.
5 Kornberg A, Blank M, Kaufman S, Shoenfeld Y. Induction of tissue factor-like activity in monocytes by anti-cardiolipin antibodies. *J Immunol* 1994; **153**: 1328–1332.
6 Atsumi T, Khamashta MA, Amengual O, Hughes GRV. Up-regulated tissue factor expression in antiphospholipid syndrome. *Thromb Haemost* 1997; **77**: 222–223.
7 Cuadrado MJ, Lopez-Pedreira C, Khamashta MA *et al.* Thrombosis in primary antiphospholipid syndrome. A pivotal role for monocyte tissue factor expression. *Arthritis Rheum* 1997; **40**: 834–841.
8 Amengual O, Atsumi T, Khamashta MA, Hughes GRV. The role of the tissue factor pathway in the hypercoagulable state in patients with the antiphospholipid syndrome. *Thromb Haemost* 1998; **79**: 276–281.
9 Khamashta MA, Harris EN, Gharavi AE *et al.* Immune mediated mechanism for thrombosis: antiphospholipid antibody binding to platelet membranes. *Ann Rheum Dis* 1988; **47**: 849–854.
10 Shechter Y, Tal Y, Greenberg A, Brenner B. Platelet activation in patients with antiphospholipid syndrome. *Blood Coagul Fibrinolysis* 1998; **9**: 653–657.
11 Hasselaar P, Derksen RH, Blokzijl L, de Groot PG. Crossreactivity of antibodies directed against cardiolipin, DNA, endothelial cells and blood platelets. *Thromb Haemost* 1990; **63**: 169–173.
12 Zhou H, Wolberg AS, Roubey RA. Characterization of monocyte tissue factor activity induced by IgG antiphospholipid antibodies and inhibition by dilazep. *Blood* 2004; **104**: 2353–2358.
13 Campbell AL, Pierangeli SS, Wellhausen S, Harris EN. Comparison of the effects of anticardiolipin antibodies from patients with the antiphospholipid syndrome and with syphilis on platelet activation and aggregation. *Thromb Haemost* 1995; **73**: 529–534.
14 Espinola RG, Pierangeli SS, Gharavi AE, Harris EN. Hydroxychloroquine reverses platelet activation induced by human IgG antiphospholipid antibodies. *Thromb Haemost* 2002; **87**: 518–522.
15 Raschi E, Testoni C, Bosisio D *et al.* Role of the MyD88 transduction signaling pathway in endothelial activation by antiphospholipid antibodies. *Blood* 2003; **101**: 3495–3500.
16 Zhang J, McCrae KR. Annexin A2 mediates endothelial cell activation by antiphospholipid/anti-beta2 glycoprotein I antibodies. *Blood* 2005; **105**: 1964–1969.
17 Meroni PL, Raschi E, Testoni C *et al.* Statins prevent endothelial cell activation induced by antiphospholipid (anti-beta2-glycoprotein I) antibodies: effect on the proadhesive and proinflammatory phenotype. *Arthritis Rheum* 2001; **44**: 2870–2878.
18 Dunoyer-Geindre S, De Moerloose P, Galve-De Rochemonteix B, Reber G, Kruithof E. NFkappaB is an essential intermediate in the activation of endothelial cells by anti-beta(2) glycoprotein 1 antibodies. *Thromb Haemost* 2002; **88**: 851–857.
19 Espinola RG, Liu X, Colden-Stanfield M, Hall J, Harris EN, Pierangeli SS. E-Selectin mediates pathogenic effects of antiphospholipid antibodies. *J Thromb Haemost* 2003; **1**: 843–848.
20 Ma K, Simantov R, Zhang JC, Silverstein R, Hajjar KA, McCrae KR. High affinity binding of beta 2-glycoprotein I to human endothelial cells is mediated by annexin II. *J Biol Chem* 2000; **275**: 15541–15548.
21 Lutters BC, Derksen RH, Tekelenburg WL, Lenting PJ, Arnout J, de Groot PG. Dimers of beta 2-glycoprotein I increase platelet deposition to collagen via interaction with phospholipids and the apolipoprotein E receptor 2'. *J Biol Chem* 2003; **278**: 33831–33838.
22 McGilvray ID, Tsai V, Marshall JC, Dackiw AP, Rotstein OD. Monocyte adhesion and transmigration induce tissue factor expression: role of the mitogen-activated protein kinases. *Shock* 2002; **18**: 51–57.
23 Ohsawa M, Koyama T, Nara N, Hirosawa S. Induction of tissue factor expression in human monocytic cells by protease inhibitors through activating activator protein-1 (AP-1) with phosphorylation of Jun-N-terminal kinase and p38. *Thromb Res* 2003; **112**: 313–320.
24 Blum S, Issbruker K, Willuweit A *et al.* An inhibitory role of the phosphatidylinositol 3-kinase-signaling pathway in vascular endothelial growth factor-induced tissue factor expression. *J Biol Chem* 2001; **276**: 33428–33434.
25 Eto M, Kozai T, Cosentino F, Joch H, Luscher TF. Statin prevents tissue factor expression in human endothelial cells: role of Rho/Rho-kinase and Akt pathways. *Circulation* 2002; **105**: 1756–1759.
26 Ono K, Han J. The p38 signal transduction pathway: activation and function. *Cell Signal* 2000; **12**: 1–13.
27 Nakajima K, Tohyama Y, Kohsaka S, Kurihara T. Protein kinase C alpha requirement in the activation of p38 mitogen-activated protein kinase,

which is linked to the induction of tumor necrosis factor alpha in lipopolysaccharide-stimulated microglia. *Neurochem Int* 2004; **44**: 205–214.

28 Vega-Ostertag M, Harris EN, Pierangeli SS. Intracellular events in platelet activation induced by antiphospholipid antibodies in the presence of low doses of thrombin. *Arthritis Rheum* 2004; **50**: 2911–2919.

29 Bohgaki M, Atsumi T, Yamashita Y *et al.* The p38 mitogen-activated protein kinase (MAPK) pathway mediates induction of the tissue factor gene in monocytes stimulated with human monoclonal anti-beta2Glycoprotein I antibodies. *Int Immunol* 2004; **16**: 1633–1641.

30 Vega-Ostertag M, Casper K, Swerlick R, Ferrara D, Harris EN, Pierangeli SS. Involvement of p38 MAPK in the up-regulation of tissue factor on endothelial cells by antiphospholipid antibodies. *Arthritis Rheum* 2005; **52**: 1545–1554.

T Koike and T Atsumi
Department of Medicine II,
Hokkaido University Graduate School of Medicine,
N15 W7, Kita-ku, Sapporo, Japan

Original Article

Expression of Inducible 6-Phosphofructo-2-Kinase/Fructose-2,6-Bisphosphatase/PFKFB3 Isoforms in Adipocytes and Their Potential Role in Glycolytic Regulation

Toshiya Atsumi,[1] Taro Nishio,[1] Hirokatsu Niwa,[1] Jun Takeuchi,[1] Hidenori Bando,[1] Chikara Shimizu,[1] Narihito Yoshioka,[1] Richard Bucala,[2] and Takao Koike[1]

6-Phosphofructo-2-kinase/fructose-2,6-bisphosphatase (PFK-2/FBPase) catalyzes the synthesis and degradation of fructose 2,6-bisphosphate (F2,6BP), which is a powerful activator of 6-phosphofructo-1-kinase, the rate-limiting enzyme of glycolysis. Four genes encode PFK-2/FBPase (PFKFB1–4), and an inducible isoform (iPFK-2/PFKFB3) has been found to mediate F2,6BP production in proliferating cells. We have investigated the role of iPFK-2/PFKFB3 and related isoforms in the regulation of glycolysis in adipocytes. Human visceral fat cells express PFKFB3 mRNA, and three alternatively spliced isoforms of iPFK-2/PFKFB3 are expressed in the epididymal fat pad of the mouse. Forced expression of the iPFK-2/PFKFB3 in COS-7 cells resulted in increased glucose uptake and cellular F2,6BP content. Prolonged insulin treatment of 3T3-L1 adipocytes led to reduced PFKFB3 mRNA expression, and epididymal fat pads from *db/db* mice also showed decreased expression of PFKFB3 mRNA. Finally, anti–phospho-iPFK-2(Ser461) Western blotting revealed strong reactivity in insulin-treated 3T3-L1 adipocyte, suggesting that insulin induces the phosphorylation of PFKFB3 protein. These data expand the role of these structurally unique iPFK-2/PFKFB3 isoforms in the metabolic regulation of adipocytes. *Diabetes* 54:3349–3357, 2005

Obesity is a strong risk factor for the development of atherosclerosis, cardiovascular disease, and metabolic disorders such as hypertriglyceridemia, hyperinsulinemia, and type 2 diabetes (1–3). Obesity occurs when energy intake exceeds energy expenditure, producing an excessive accumulation of fat tissue, which is composed of adipocytes. Adipose tissue also is considered to be an important regulatory organ for systemic glucose and fat metabolism and for overall energy balance. Adipose tissue uses glucose for the synthesis of fat; in particular, the glycolytic product, glycerol 3-phosphate, is a precursor for the synthesis of triacylglycerols. The precise mechanisms governing glycolytic flux and triacylglycerol synthesis under normal and pathological circumstances remain incompletely understood.

Fructose 2,6-bisphosphate (F2,6BP) is a potent allosteric activator of phosphofructokinase-1 (PFK-1), which is a rate-limiting enzyme of glycolysis (4–7). The synthesis and degradation of F2,6BP is regulated by the bi-functional enzyme, 6-phosphofructo-2-kinase/fructose-2,6-bisphosphatase (PFK-2/FBPase) (8). Four distinct genes have been reported to encode PFK-2/FBPase (PFKFB1, PFKFB2, PFKFB3, and PFKFB4) (4), and each isoform differs in its kinase and phosphatase activities, its tissue distribution, and its regulatory response to protein kinases. Tissue-specific enzyme isoforms are a means to tightly regulate the metabolic demands of a particular tissue. In the case of PFK-2/FBPase, it is known that the PFKFB3 gene product has a high kinase–to–phosphatase activity ratio that serves to maintain elevated F2,6BP levels and thereby sustain a high glycolytic rate (9–11). Liver PFK-2/PFKFB1, by contrast, is a substrate for a cAMP-dependent protein kinase A that phosphorylates Ser32, leading to an inactivation of the kinase domain and an activation of the phosphatase domain (12,13). This regulatory mechanism accounts for the inhibitory effect of glucagon on glycolysis in the liver. PFKFB3 lacks the serine phosphorylation site for protein kinase A and does not show this liver-associated feature of regulatory control (9).

iPFK-2 is a recently described PFK-2 isoform that is encoded by the PFKFB3 gene on human chromosome 10. iPFK-2/PFKFB3 is expressed in rapid proliferating cells, such as tumor cells, epithelial cells, and activated immune cells (11,14), and it is distinguished by the presence of an oncogene-like, AUUUA regulatory sequence in the 3′ untranslated region (UTR) of its mRNA. The AUUUA motif confers instability and enhanced translational activity to mRNAs, and it typifies the 3′ UTR structure of several proto-oncogenes and proinflammatory cytokines (15). iPFK-2/PFKFB3 is phosphorylated on Ser461 by the regulatory kinase, AMP-activated protein kinase (16). This modification further increases the conversion of F6P to F2,6BP, and it appears consistent with the role of this enzyme in metabolic activation and cell proliferation.

From the [1]Department of Medicine II, Graduate School of Medicine, Hokkaido University, Sapporo, Japan; and the [2]Department of Medicine and Pathology, School of Medicine, Yale University, New Haven, Connecticut.

Address correspondence and reprint requests to Toshiya Atsumi, MD, PhD, Department of Medicine II, Hokkaido University Graduate School of Medicine, kita 15, Nishi 7, kita-ku, Sapporo 060-8638, Japan. E-mail: tatsumi@med.hokudai.ac.jp.

Received for publication 29 November 2004 and accepted in revised form 29 August 2005.

DMEM, Dulbecco's modified Eagle's medium; F2,6BP, fructose 2,6-bisphosphate; FBS, fetal bovine serum; IBMX, 3-isobutyl-1-methylxanthine; IRS, insulin receptor substrate; PFK-1, phosphofructokinase-1; PFK-2/FBPase, 6-phosphofructo-2-kinase/fructose-2,6-bisphosphatase; PPAR, peroxisome proliferator–activated receptor; UTR, untranslated region.

Alternative splicing of the variable, COOH-terminal region of the PFKFB3 gene can lead to the expression of six structural isoforms in human brain (17). Although these isoforms have been reported to differ in the structure of their COOH termini, their precise physiological roles are unknown. In the present report, we have explored the expression and activity of different PFKFB3 isoforms in adipose tissue with the goal of initiating an investigation of the potential role of these enzymes in the metabolic changes underlying obesity.

RESEARCH DESIGN AND METHODS

Insulin, dexamethazone, and 3-isobutyl-1-methylxanthine (IBMX) were obtained from Sigma-Aldrich (St. Louis, MO). Troglitazone was a gift from Sankyo (Tokyo, Japan). A rabbit polyclonal anti–phospho-iPFK-2(Ser461) antibody was raised against the phosphorylated peptide RRN(Sp)VTP (corresponding to residues 458–463 of human iPFK-2 in which Ser461 was phosphorylated) (18). Goat polyclonal antibody (anti–PFK-2 br/pl N-11 antibody), which reacts with the mouse iPFK-2/PFKFB3 isoform, was purchased from Santa Cruz Biotechnology (Santa Cruz, CA). Formalin-fixed, paraffin-embedded human fat tissue was obtained from Novagen (Madison, WI).

3T3-L1 cells and COS-7 cells were obtained from American Type Cell Culture (Manassas, VA). Cells were grown in Dulbecco's modified Eagle's medium (DMEM) (Life Technologies, Grand Island, NY) supplemented with 10% heat-inactivated fetal bovine serum (FBS) (HyClone Laboratories, Logan, UT) at 37°C in a humidified 5% CO_2 incubator. For adipocyte differentiation, 3T3-L1 cells were stimulated after 2 days of confluence with 10 μg/ml insulin, 0.5 mmol/l IBMX, and 1.0 μmol/l dexamethazone. After 48 h, the medium was replaced with DMEM supplemented with 10% FBS. Fresh medium was added every 48 h.

C57BL/KsJ-*db*/*db* Jcl mice and C57BL/KsJ-+m/+m Jcl mice were obtained from CLEA Japan (Tokyo, Japan). This study was approved by the Animal Experiment Ethics Committee of the Graduate School of Medicine of Hokkaido University.

In situ hybridization. PFKFB3 is distinguished from other members of the PFKFB family by the presence of AU-rich element in 3′ UTR of its mRNA. Therefore, we designed a specific probe for PFKFB3 mRNA that included the AU-rich element. The procedure of in situ hybridization is described in a previous report (14).

Cloning of the mouse adipocyte PFKFB3. Epididymal fat pads from male C57BL/6 mouse (10 weeks of age) were harvested and frozen in liquid nitrogen. The frozen tissue was homogenized, and the total RNA was extracted using the RNeasy Lipid Tissue Midi kit (Qiagen, Valencia, CA). One microgram total RNA was reverse transcribed with Omniscript Reverse Transcriptase (Qiagen) in a 20-μl reaction mixture using oligo-d$(T)_{12-18}$ primer (Invitrogen, Carlsbad, CA). Full-length mouse adipocyte cDNA was amplified with specific primers coding for mouse PFKFB3 (5′-ATGCCGTTGGAACTGA CCCA-3′ and 5′-GTGCTTCTGGGAAGAGTCGGCAC-3′; GenBank accession no. AF294617). PCR was carried out with Advantage 2 PCR Enzyme System (BD Biosciences Clontech, Palo Alto, CA) according to the manufacturer's protocol. PCR products were separated by electrophoresis on a 2% agarose gel and purified using a GENECLEAN (Qbiogene, Carlsbad, CA). The PCR products then were cloned into the pcDNA3.1/V5-His vector and transformed into TOP10 *Escherichia coli* cells. Purified plasmid DNA was sequenced bi-directionally using the BigDye Terminator cycle sequencing kit (Applied Biosystems, Foster City, CA). The sequencing reaction products were analyzed with the ABI Model 373A DNA sequencer (Applied Biosystems).

Western blot analysis. Cells were washed in ice-cold PBS and then radioimmunoprecipitation assay buffer containing 150 mmol/l NaCl, 1% Nonidet P-40, 0.5% doxycholate, 0.1% SDS, and 50 mmol/l Tris (pH 7.5) with protease inhibitors (Complete, Mini, and EDTA-free; Roche Diagnostics, Indianapolis, IN). The samples were mixed with an equal volume of 2× Laemmli sample buffer and were denatured for 5 min at 85°C. The proteins were separated on 10% SDS-polyacrylamide electrophoresis gels (Bio-Rad, Hercules, CA) and transferred to polyvinylidene difluoride membranes (Millipore, Bedford, MA). The membranes were incubated with a polyclonal anti–phospho-iPFK-2(Ser461) antibody (1:1,000), and the bound antibody was visualized with horseradish peroxidase–conjugated donkey anti-rabbit antibody and chemiluminescence (ECL system; Amersham, Buckinghamshire, U.K.).

RT-PCR. Total RNA was extracted using the RNeasy Mini kit (Qiagen) according to the manufacturer's protocol. One microgram total RNA was reverse transcribed with Omniscript Reverse Transcriptase (Qiagen) in a 20-μl reaction mixture using oligo-d$(T)_{12-18}$ primer. PCR was carried out with the Platinum PCR SuperMix (Invitrogen). For the amplification of the variable region of PFKFB3 cDNA, 200 mmol/l forward primer (5′-ATTTACTTGAATGT AGAATCGGTGAG-3′) and the reverse primer (5′-TCAGTGTTTCCTGGAGGA GTCAGC-3′) were used. The PCR conditions were initial denaturation for 3 min at 95°C; 38 cycles of 30 s at 95°C, 30 s at 61°C, and 1 min at 72°C; and finally 10 min at 72°C. The PCR products were separated by electrophoresis on a 5% polyacrylamide gel. PCR was performed in a Perkin-Elmer model 2400 thermal cycler (Applied Biosystems). In accordance with the previous findings, the length of the resultant PCR product enable us to distinguish between the different PFKFB3 splicing variants. Amplified fragments from each PCR were cloned into pCR2.1 vector (Invitrogen) and sequenced using the dye terminator cycle sequence kit (Applied Biosystems).

Quantitative real-time RT-PCR. Quantitative real-time RT-PCR for PFKFB3 mRNA was performed using the ABI 7000 Sequence Detector (Applied Biosystems) using a QuantiTect SYBR green RT-PCR kit (Qiagen). The following primers were used for specific amplification for mouse PFKFB3, 5′-AGAACTTCCACTCTCCCACCCAAA-3′ and 5′-AGGGTAGTGCCCATTGTTG AAGGA-3′ (GenBank accession no. AF294617). The specificity of each PCR product was routinely checked by melting curve analysis and by agarose gel electrophoresis.

Northern blot analysis. As described before, PFKFB3 is distinguished by the presence of AU-rich element in its 3′ UTR. Therefore, mouse PFKFB3 3′ UTR containing the AUUUA motif (corresponding to mouse PFKFB3 3669–4398) was cloned into the pCRII vector (Invitrogen), and antisense RNA probes were synthesized with the DIG RNA Labeling kit (Roche Diagnostics). This probe is specific for PFKFB3 and does not react with other members of the PFKFB family. Northern blot procedures are described in the previous report (14).

Transfection of COS-7 cells. Cells were cultured in 6-well plates in DMEM/10% FBS and transfected PFKFB3 in pcDNA3.1/V5-His vector using a FuGENE6 reagent (Roche Diagnostics) according to the manufacturer's protocol. After 48 h, the cells were used for experiments. The expression of recombinant protein was confirmed by Western blotting using an anti-V5 antibody, which recognizes short amino acid sequences fused to the recombinant gene within the cloning vector.

Glucose transport assay. Cells plated in 6-well culture dishes were washed with glucose transport solution (140 mmol/l NaCl, 20 mmol/l HEPES/Na, 5 mmol/l KCl, 2.5 mmol/l $MgSO_4$, and 1 mmol/l $CaCl_2$) and incubated for 10 min with 2-deoxy-[^{3}H]glucose. The cells then were washed three times with transport solution and lysed with 0.8 ml 50 mmol/l NaOH. The lysates then were collected, and the radioactivity was measured by scintillation counting.

Measurement of F2,6BP. Intracellular F2,6BP content was measured using Van Schaftingen's method after the disruption of cells in 0.8 ml 50 mmol/l NaOH (8).

Statistical analysis. Results are expressed as means ± SD. Statistical significance of difference was assessed by Student's *t* test.

RESULTS

Detection of PFKFB3 mRNA in human visceral fat tissue. To examine the expression of PFKFB3 mRNA in human visceral fat, we designed an RNA probe that was complementary to the 3′ UTR, including the AU-rich element, of PFKFB3 and developed an in situ hybridization method. This probe is specific for PFKFB3 mRNA and does not cross-react with other members of the PFKFB family (14). We also confirmed the detection of a single, expected band corresponding to the PFKFB3 5.4-kb mRNA using this probe in Northern blot analysis of different human tumor tissues (data not shown). As shown in Fig. 1, PFKFB3 mRNA is readily detectable within adipocytes, and no cell-associated signals were detected with the PFKFB3 sense probe.

Cloning of the PFKFB3 from mouse adipose tissue. A previous report has provided evidence for six distinct isoforms of the PFKFB3 gene product in human brain (17). Alternatively spliced isoforms of PFK-2/FBPase also were reported in a study of the rat brain (19,20). To examine the expression pattern of the PFKFB3 in mouse adipocytes, total RNA was extracted from mouse (C57BL/6) epididymal fat pads, the cDNA was synthesized by reverse transcriptase, and the PFKFB3 cDNA was amplified and cloned into the pcDNA3.1/V5-His vector. Three different isoforms thus were identified, designated PFKFB3-ABCG,

FIG. 1. Analysis of PFKFB3 mRNA expression in human visceral fat. *A*: Tissue sections were examined by hematoxylin and eosin. Tissue sections were examined by in situ hybridization using antisense RNA probe (*B*) and sense RNA probe (*C*). Magnification ×400.

PFKFB3-ACG, and PFKFB3-AG (Fig. 2*A*). These sequences differ in the predicted structure of their COOH termini and in their overall exonic organization. The variable region of COOH termini of PFKFB3 in human and rat brain is derived from seven exons, as described previously, whereas the 3′-variable region of mouse adipocyte PFKFB3 is encoded by four exons (Fig. 2*B*). The structures of exons A, C, and G in mouse PFKFB3 gene are homologous to those of the rat and human PFKFB3 gene. The shortest isoform, PFKFB3-AG, contains exons A and G. The exon-intron structure of PFKFB3-AG has not been identified in rat brain, but it has been described in human brain PFK-2 (17).

The expression of PFKFB3 isoforms are induced during 3T3-L1 adipocyte differentiation. Numerous genes are induced as part of the adipocyte differentiation program. We next investigated the expression of PFKFB3 in cultured mouse 3T3-L1 cells induced to undergo adipocyte differentiation. We designed specific primers for amplification of PFKFB3 and an antisense RNA probe that is specific for PFKFB3 mRNA 3′ UTR, as described in RESEARCH DESIGN AND METHODS. Quantitative real-time RT-PCR

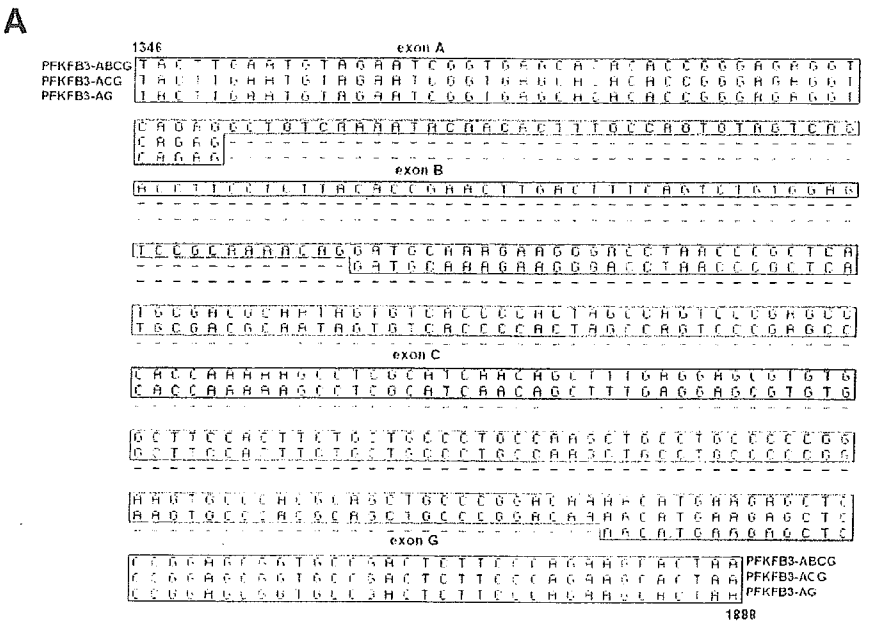

FIG. 2. Comparison of the COOH-terminal variable regions of the mouse PFKFB3 in adipocytes. Alignment analysis of the nucleotide sequences of different PFKFB3 isoforms in mouse adipocytes. The alignment is shown downstream of the nucleotide 1346 of the mouse PFKFB3. Residues within the solid boxes indicate identities. *A*: Gaps are shown as dashes. *B*: Schematic diagram shows the intron-exon organization of the variable region of the mouse PFKFB3 in adipocytes.

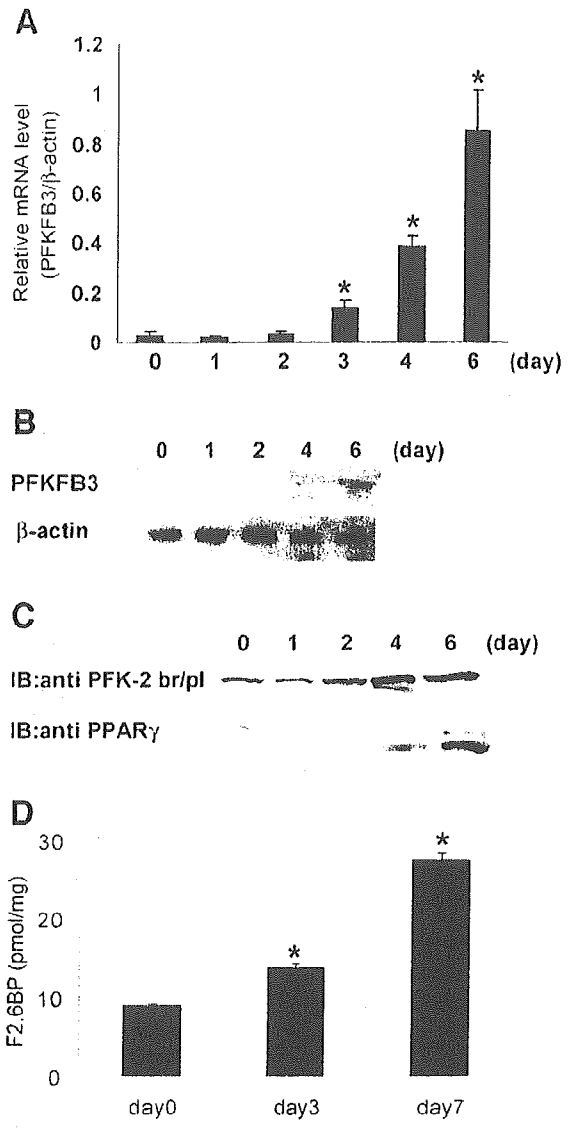

FIG. 3. The expression of PFKFB3 during 3T3-L1 adipocyte differentiation. Quantitative real-time RT-PCR using specific primer for PFKFB3 (*A*) and Northern blotting using specific probe for PFKFB3 (*B*). *C*: Western blotting using anti-PFK-2 br/pl antibody. Intracellular F2,6BP was measured as described in RESEARCH DESIGN AND METHODS. *D*: Each point represents the means ± SD of three different samples. $^*P < 0.05$ compared with the control value. IB, immunoblot.

analysis and Northern blot analysis of 3T3-L1 cells showed that the expression of PFKFB3 mRNA was significantly increased during differentiation (Fig. 3*A* and *B*). Because of the low sensitivity of antisense RNA probe used in Northern blot analysis, which is unavoidable given the close sequence homology among the different isoforms, the induction of PFKFB3 mRNA in day 4 is not clearly defined by Northern blotting. Nevertheless, there is clear and apparent induction of PFKFB3 mRNA observed by real-time RT-PCR analysis. As shown in Fig. 3*C*, the production of PFKFB3 protein increased during adipocyte differentiation, as assessed by Western blot analysis. The induction and increase in the level of PFKFB3 protein was similar to that observed for peroxisome proliferator–activated receptor (PPAR)-γ, which is a well-characterized feature of adipocyte differentiation. Intracellular F2,6BP levels also increased significantly during adipocyte differentiation (Fig. 3*D*).

The expression pattern of splicing variants for PFKFB3 during 3T3-L1 adipocyte differentiation. We analyzed the expression pattern of the splicing variants of PFKFB3 during 3T3-L1 adipocyte differentiation by RT-PCR analysis. As described in the RESEARCH DESIGN AND METHODS, we selected a forward primer that was complementary to a sequence in the constant region of PFKFB3 cDNA and a reverse primer that was located close to the stop codon (17). Amplification with these primer pairs revealed three PCR products of sizes 345, 270, and 96 bp that correspond to the designated PFKFB3 isoforms: PFKFB3-ABCG, PFKFB3-ACG, and PFKFB3-AG. Sequence analysis also confirmed that each isoform contained the COOH-terminal variable region of PFKFB3 (data not shown). The expression of these isoforms, in particular PFKFB3-ACG and PFKFB3-AG, was significantly increased during 3T3-L1 adipocyte differentiation (Fig. 4). Taken together, these findings indicate that the increase in glycolytic flux that accompanies adipocyte differentiation is associated with PFK-2 expression: an increase in the level of the mRNAs for PFKFB3 and in particular the PFKFB3-ACG and PFKFB3-AG.

Troglitazone induces the expression of PFKFB3 mRNA and protein in 3T3-L1 cells. Thiazolidinedione is a ligand for PPAR-γ (21), and it increases the number of small adipocytes in white adipose tissue (22). We examined the effect of troglitazone, one of thiazolidinediones, on the expression of iPFK-2/PFKFB3 in 3T3-L1 cells. As shown in Fig. 5*A* and *B*, the expression of PFKFB3 mRNA increases after treatment of troglitazone, as analyzed by quantitative real-time RT-PCR analysis and Northern blotting, and this finding is accompanied by a corresponding increase in immunoreactive PFKFB3 protein (Fig. 5*C*). The induction and increase in the level of PFKFB3 expression was similar to that observed for PPAR-γ, suggesting a potential role for PFKFB3 in the regulation of glycolysis during triacylglycerol synthesis. We also examined the expression of different splicing variants of PFKFB3 in 3T3-L1 cells stimulated with troglitazone. As shown in Fig. 5*D*, the expression of PFKFB3-ABCG, PFKFB3-ACG, and PFKFB3-AG also increased after the administration of troglitazone.

Overexpression of the PFKFB3 results in increased glycolysis. To validate the enzymatic activity and potential physiological role of PFKFB3-ACG and PFKFB3-AG in glycolytic flux, we cloned both isoforms into the pcDNA3.1/V5-His vector and transfected them into COS-7 cells. Transfection efficiencies were calculated by determining the number of transfected cells using β-Gal staining kit (Invitrogen), and 70% of COS-7 cells expressed reporter gene protein. Transfection of each isoform in COS-7 cells resulted in a significant increase in PFKFB3 protein, as revealed by Western blot analysis using an anti-V5 antibody, which recognizes the short amino acid sequence fused to the recombinant gene encoded within the cloning vector (Fig. 6*A*). Overexpression of PFKFB3 protein also was confirmed by Western blot analysis using an anti–PFK-2 br/pl antibody. PFKFB3-ACG and PFKFB3-AG were expressed in equivalent levels in the COS-7 transfection system. As mentioned previously, iPFK-2/PFKFB3 is phosphorylated at the Ser461 residue, which is located in exon C of COOH-terminal variable region. Accordingly, immunoblotting with an anti–phospho-iPFK-2(Ser461) anti-

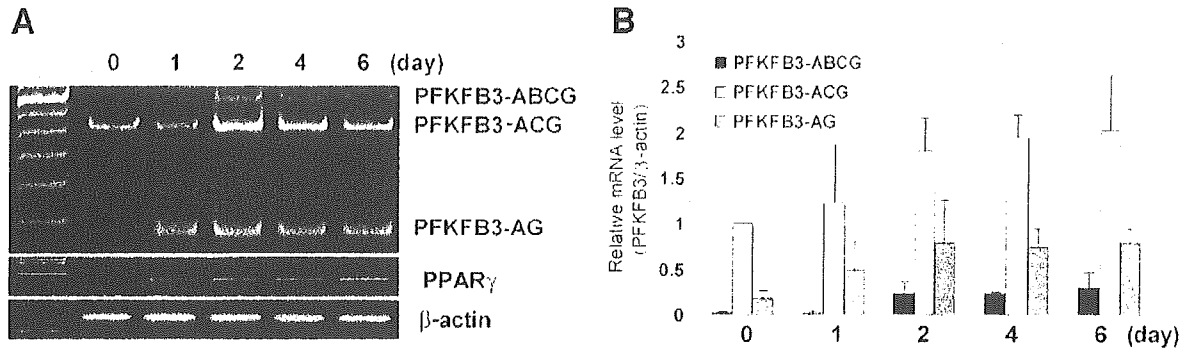

FIG. 4. The expression pattern of splicing variants of PFKFB3 during 3T3-L1 adipocyte differentiation. PCR amplification reactions were carried out across the variable region of PFKFB3. *A*: The PCR products were separated by electrophoresis on a 5% polyacrylamide gel and stained with ethidium bromide. *B*: Densitometric analysis of the expression of mRNA for PFKFB3 isoforms during 3T3-L1 adipocyte differentiation. Values are means ± SD for three different samples.

body revealed a prominent band corresponding to the 60-kDa iPFK-2/PFKFB3 in the lysates of COS-7 cells expressing PFKFB3-ACG but at significantly reduced levels in COS-7 cells transfected with an PFKFB3-AG. The intracellular content of F2,6BP was significantly increased after transfection by both isoforms (Fig. 6*B*). Note that COS-7 cells express endogenous PFKBF3, which is normally phosphorylated under serum culture conditions (18). The uptake of 2-deoxyglucose into cells also was increased in both cases, indicating that the increased production of these proteins produced a physiologically meaningful increase in glycolytic flux (Fig. 6*C*).

Prolonged insulin stimulation results in a reduction of PFKFB3 mRNA. The physiological impact of insulin on glucose metabolism changes critically with the duration of stimulation of the insulin receptor. We next examined the effect of prolonged insulin treatment on the expression of PFKFB3 mRNA in differentiated adipocytes. 3T3-L1 adipocytes were treated with insulin for 18 h, and the expression of PFKFB3 mRNA was measured by quantitative real-time RT-PCR analysis. As shown in Fig. 7*A*, the expression of PFKFB3 mRNA in 3T3-L1 adipocytes decreased significantly after long-term insulin stimulation, whereas similar conditions caused no significant change of PFKFB3 mRNA expression in 3T3-L1 preadipocytes, which have less insulin binding activity and less insulin receptor expression when compared with 3T3-L1 adipocytes (data not shown) (23,24). These data suggest a cell-specific mode of regulation of the expression of PFKFB3 mRNA by insulin in adipocytes.

Mice of the genotype *db/db* have a point mutation in the leptin receptor gene, and they are an established model of type 2 diabetes (25). We next examined the expression of PFKFB3 mRNA in epididymal fat pads obtained from *db/db* mice. We found that the expression of PFKFB3 mRNA was significantly reduced in the fat pads of *db/db* mice analyzed by quantitative real-time RT-PCR (Fig. 7*B*). The expression of PFKFB3 protein in adipose tissue was not significantly different between the *db/db* mice and control mice (data not shown).

Insulin-induced serine phosphorylation of iPFK-2/PFKFB3 isoforms in 3T3-L1 adipocytes. Insulin action is initiated by hormone binding to cell-surface insulin receptors, leading to the tyrosine phosphorylation of several intracellular mediators and downstream metabolic effects (26–29). Monocyte activation is known to occur by a glucose-dependent mechanism, and it is associated with an increase in iPFK-2 protein production and its phosphorylation (16,30–32). We next examined the ability of insulin to phosphorylate PFKFB3 isoforms in cultured adipocytes. The contribution of the phosphorylation of the COOH-terminal serine to the kinetic properties of PFK-2 is well-characterized in the cardiac, PFK-2 isoform. The insulin-induced increase in F2,6BP and heart PFK-2 activity occurs by the phosphorylation of the serine residues, Ser466 and Ser483 (33). Protein kinase B phosphorylates substrates at Ser/Thr in a conserved motif characterized by Arg at position −5 and −3. The amino acid sequences surrounding Ser466 of heart PFK-2 and Ser461 of iPFK-2/PFKFB3 are similar, although iPFK-2/PFKFB3 lacks Arg at position −5. In addition, Ser466 of heart PFK-2 can be phosphorylated in vitro and in vivo by a number of protein kinases (34). We hypothesized that its phosphorylation may similarly upregulate the kinase activity of iPFK-2/PFKFB3 protein. We generated anti–phospho-iPFK-2 (Ser461) antibody as described in RESEARCH DESIGN AND METHODS. Serum-starved, 3T3-L1 adipocytes were exposed to insulin for 5 min, and the proteins from cell extract were separated by SDS-PAGE. The phosphorylation of PFKFB3 isoforms was examined by Western blot analysis using recently characterized anti—phospho-iPFK-2(Ser461)–specific antibody (18). Insulin significantly increased the serine phosphorylation of iPFK-2/PFKFB3 isoforms (Fig. 8*A*). Intracellular F2,6BP content increased in parallel with the phosphorylation of PFKFB3 isoforms (Fig. 8*B*). These data suggest that increased glycolytic flux induced by insulin in 3T3-L1 adipocytes is mediated by phosphorylation of PFKFB3 at position Ser461.

DISCUSSION

Insulin stimulates glucose transport via tyrosine phosphorylation of the insulin receptor and insulin receptor substrates (IRSs), leading to the downstream activation of phosphatidylinositol 3-kinase (35). The precise mechanisms responsible for the activation of glycolytic enzymes by insulin are of significant interest. Insulin has been shown to increase intracellular F2,6BP content by activating kinase activity of PFK-2/FBPase in adipocytes (36), but the particular enzymatic isoforms of PFK-2/FBPase that mediate increased glycolytic flux and triacylglycerol synthesis are unknown.

In the present study, we identify PFKFB3 as the isoform that is likely responsible for the activation of glycolysis in

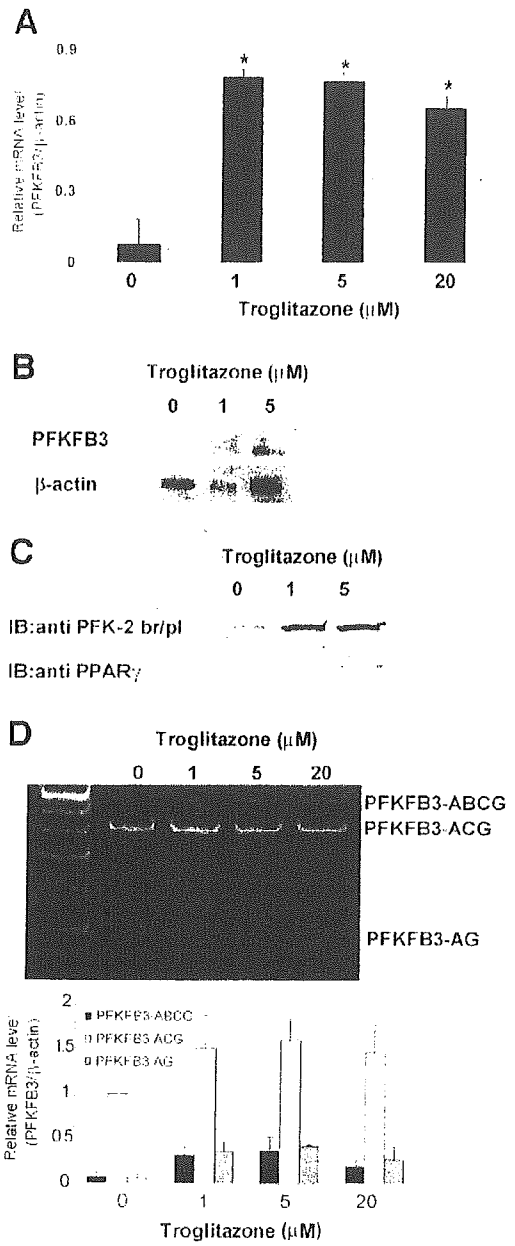

FIG. 5. The effect of troglitazone on the expression of PFKFB3 mRNA and protein. Quantitative real-time RT-PCR (*A*) and Northern blotting (*B*). Western blotting using an anti–PFK-2 br/pl antibody (*C*). RT-PCR analysis of splicing variants of PFKFB3 mRNA (*D*). Values are means ± SD for three different samples. $*P < 0.05$ compared with the control value.

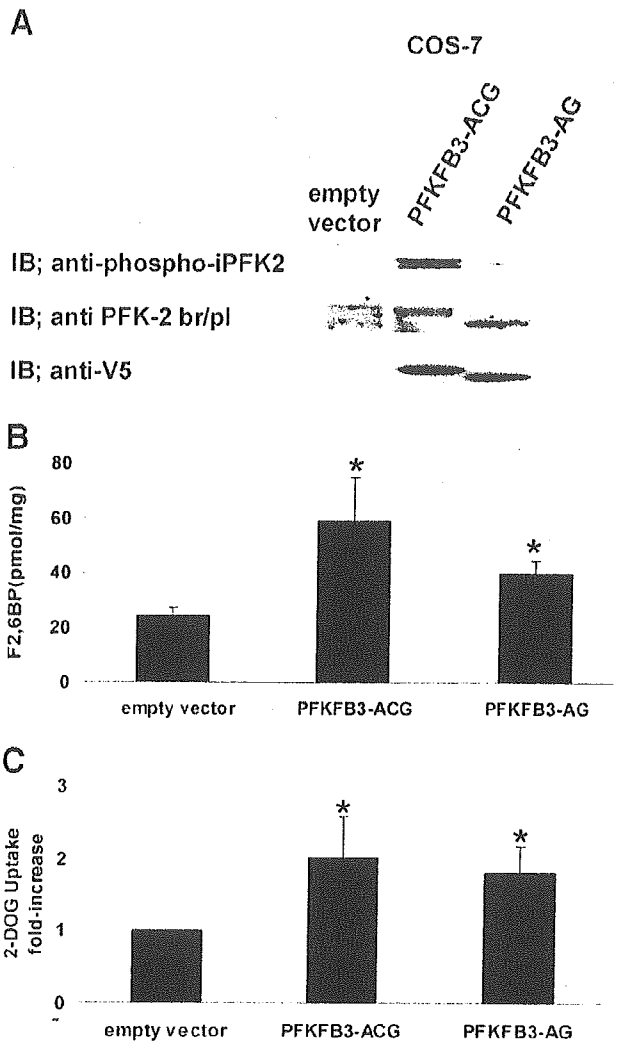

FIG. 6. Effect of forced expression of the recombinant PFKFB3 protein. *A*: Western blot analysis of COS-7 cells transfected with plasmids encoding PFKFB3-ACG or PFKFB3-AG was carried out using anti-phospho-iPFK-2(Ser461) antibody, PFK-2 br/pl antibody, and anti-V5 antibody. Intracellular F2,6BP content (*B*) and 2-deoxyglucose (2-DOG) uptake (*C*) were detected as described in RESEARCH DESIGN AND METHODS. $*P < 0.05$ compared with the control value. IB, immunoblot.

adipocytes. Several lines of evidence support this conclusion. The expression of PFKFB3 mRNA in human visceral fat was confirmed by in situ hybridization, and the expression of both PFKFB3 mRNA and protein was significantly increased during 3T3-L1 adipocyte differentiation induced by insulin, dexamethazone, and IBMX. Further support for this observation is offered by the report that the PFKFB3 is induced by cyclic-AMP-dependent protein kinase signal activation (37). Troglitazone stimulated the induction of PFKFB3 mRNA and PFKFB3 protein expression in 3T3-L1 cells. Moreover, insulin stimulation was associated with phosphorylation of Ser461 residue of PFKFB3 protein. We also observed the coordinate expression of the PFKFB3-ACG and the PFKFB3-AG isoforms during 3T3-L1 adipocyte differentiation, and we confirmed the potential enzymatic activity of these isoforms by transfection studies in COS-7 cells.

Marsin et al. (16) recently demonstrated that the mechanism of the activation of iPFK-2/PFKFB3 involves phosphorylation of Ser461 residue in the COOH-terminal region by AMP-activated protein kinase. The contribution of this phosphorylation event to the kinetic properties of PFK-2 has been well-characterized in heart PFK-2 (33,38–40). However, the expression of heart PFK-2/PFKFB2 in adipocytes is low when compared with iPFK-2/PFKFB3. The expression of the heart PFK-2/PFKFB2 isoform also is not induced during adipocyte differentiation (data not shown), whereas the mRNA for PFKFB3 is significantly increased during this process. These data, taken together, are con-

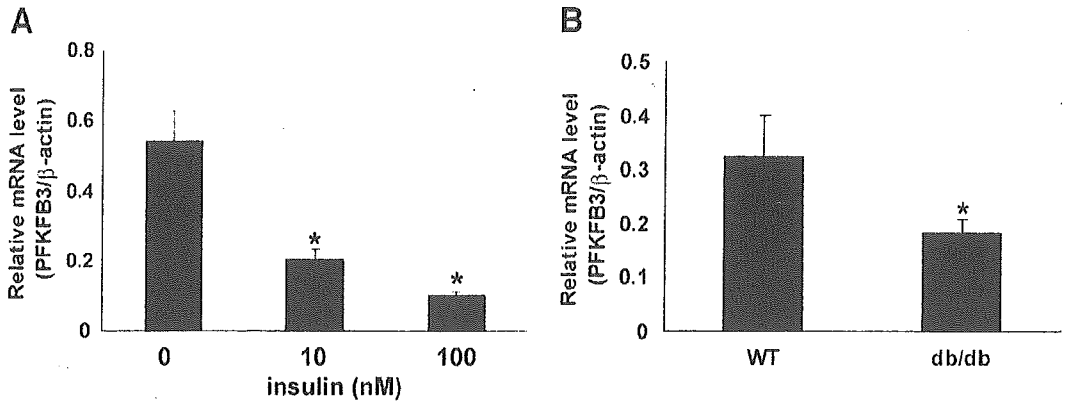

FIG. 7. *A*: The effect of prolonged stimulation by insulin on the expression of PFKFB3 mRNA in 3T3-L1 adipocytes was analyzed by quantitative real-time RT-PCR. *B*: Quantitative real-time RT-PCR analysis of the expression of PFKFB3 in the epididymal fat pad of *db/db* mice. Values are the means ± SD for three different samples. $^*P < 0.05$ compared with the control value.

sistent with an important role for PFKFB3 in the synthesis of triacylglycerols in adipocytes.

The protein kinase that is responsible for the phosphorylation of Ser461 of iPFK-2/PFKFB3 has not been clarified. The Ser461 residue of brain PFK-2/PFKFB3 (which may be alternatively numbered as Ser460) is reported to be phosphorylated by protein kinase B and other protein kinases but without activation of PFK-2 in vitro (41). Instead, phosphorylation of Ser460 decreased the sensitivity of the PFK-2 to the potent allosteric inhibitor, phosphoenolpyruvate (41). These data support the notion that phosphorylation of the PFKFB3 protein regulates PFK-2 activity, which is important for glycolytic flux.

Chronic insulin treatment has been shown to decrease the half-life of IRS-1, which is consistent with a regulatory effect on IRS-1 protein degradation. We hypothesize that the expression of PFKFB3 mRNA in the fat tissue of *db/db* mice increases during adipogenesis and that a reduction of

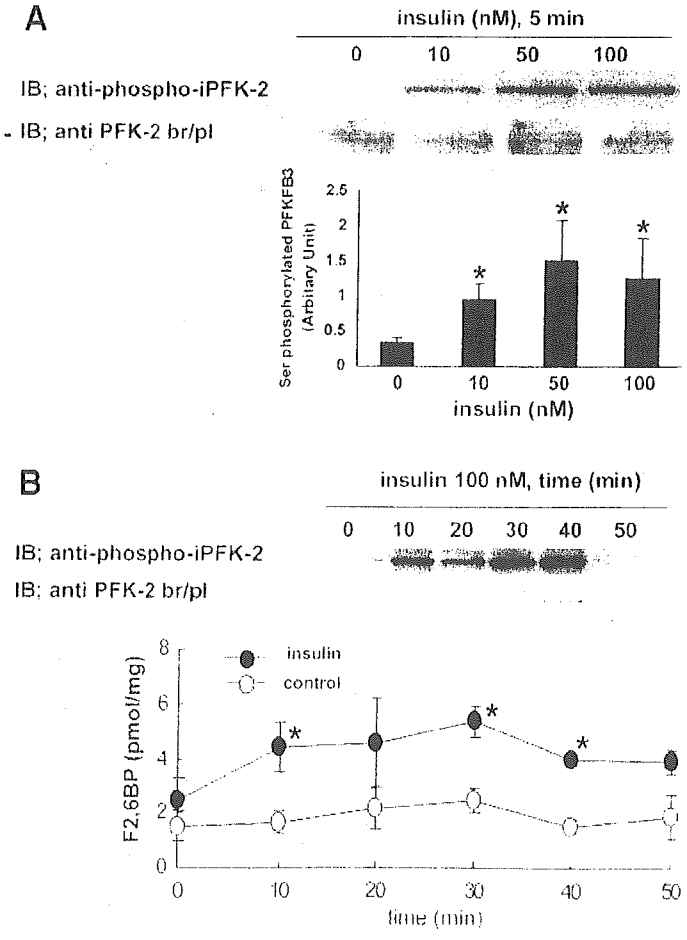

FIG. 8. The effect of insulin on the serine phosphorylation of PFKFB3. Western blotting using anti–phospho-iPFK-2(Ser461) antibody. *A*: The bar graph represents quantitative analysis of the results means ± SD for three different samples. *B*: Time-dependent changes in phosphorylation of PFKFB3 in 3T3-L1 adipocytes incubated with insulin and F2,6BP levels determined as described in RESEARCH DESIGN AND METHODS. Each point represents the means ± SD of three independent experiments. $^*P < 0.05$ compared with the control value. IB, immunoblot.

PFKFB3 mRNA may then occur after prolonged hyperglycemia as a result of a negative feedback mechanism involving insulin. This is supported by the fact that prolonged treatment by insulin causes a reduction in the expression of PFKFB3 mRNA in 3T3-L1 adipocytes. Injection of insulin to fed rats has been shown to decrease F2,6BP content in white adipose tissue; however, such a decrease was not observed in fat pads from starved rats (42). These observations are consistent overall with the notion that the accumulation of F2,6BP via insulin in adipose tissue is regulated by negative feedback system.

In conclusion, we have identified the PFKFB3 structural isoform to be a potential regulator of glycolytic flux in adipocytes. The tissue-specific regulation of the expression and phosphorylation of PFKFB3 may represent novel targets for the treatment of metabolic disorders related to obesity.

ACKNOWLEDGMENTS

R.B. has received National Institutes of Health grants 2-R01-AI-423101 and 1-RO1-AR-49610.

REFERENCES

1. Larsson B: Obesity, fat distribution and cardiovascular disease. *Int J Obes* 15 (Suppl. 2):53–57, 1991
2. Bjorntorp P: Abdominal fat distribution and disease: an overview of epidemiological data. *Ann Med* 24:15–18, 1992
3. DeFronzo RA, Ferrannini E: Insulin resistance: a multifaceted syndrome responsible for NIDDM, obesity, hypertension, dyslipidemia, and atherosclerotic cardiovascular disease. *Diabetes Care* 14:173–194, 1991
4. Okar DA, Manzano A, Navarro-Sabate A, Riera L, Bartrons R, Lange AJ: PFK-2/FBPase-2: maker and breaker of the essential biofactor fructose-2,6-bisphosphate. *Trends Biochem Sci* 26:30–35, 2001
5. Van Schaftingen E: Fructose 2,6-bisphosphate. *Adv Enzymol Relat Areas Mol Biol* 59:315–395, 1987
6. Hue L, Rider MH: Role of fructose 2,6-bisphosphate in the control of glycolysis in mammalian tissues. *Biochem J* 245:313–324, 1987
7. Pilkis SJ, Claus TH, Kurland IJ, Lange AJ: 6-Phosphofructo-2-kinase/fructose-2,6-bisphosphatase: a metabolic signaling enzyme. *Annu Rev Biochem* 64:799–835, 1995
8. Hue L, Rousseau GG: Fructose 2,6-bisphosphate and the control of glycolysis by growth factors, tumor promoters and oncogenes. *Adv Enzyme Regul* 33:97–110, 1993
9. Sakakibara R, Kato M, Okamura N, Nakagawa T, Komada Y, Tominaga N, Shimojo M, Fukasawa M: Characterization of a human placental fructose-6-phosphate, 2-kinase/fructose-2,6-bisphosphatase. *J Biochem (Tokyo)* 122:122–128, 1997
10. Riera L, Manzano A, Navarro-Sabate A, Perales JC, Bartrons R: Insulin induces PFKFB3 gene expression in HT29 human colon adenocarcinoma cells. *Biochim Biophys Acta* 1589:89–92, 2002
11. Chesney J, Mitchell R, Benigni F, Bacher M, Spiegel L, Al-Abed Y, Han JH, Metz C, Bucala R: An inducible gene product for 6-phosphofructo-2-kinase with an AU-rich instability element: role in tumor cell glycolysis and the Warburg effect. *Proc Natl Acad Sci U S A* 96:3047–3052, 1999
12. Pilkis SJ, El-Maghrabi MR, Coven B, Claus TH, Tager HS, Steiner DF, Keim PS, Heinrikson RL: Phosphorylation of rat hepatic fructose-1,6-bisphosphatase and pyruvate kinase. *J Biol Chem* 255:2770–2775, 1980
13. El-Maghrabi MR, Noto F, Wu N, Manes N: 6-Phosphofructo-2-kinase/fructose-2,6-bisphosphatase: suiting structure to need, in a family of tissue-specific enzymes. *Curr Opin Clin Nutr Metab Care* 4:411–418, 2001
14. Atsumi T, Chesney J, Metz C, Leng L, Donnelly S, Makita Z, Mitchell R, Bucala R: High expression of inducible 6-phosphofructo-2-kinase/fructose-2,6-bisphosphatase (iPFK-2; PFKFB3) in human cancers. *Cancer Res* 62:5881–5887, 2002
15. Shaw G, Kamen R: A conserved AU sequence from the 3′ untranslated region of GM-CSF mRNA mediates selective mRNA degradation. *Cell* 46:659–667, 1986
16. Marsin AS, Bouzin C, Bertrand L, Hue L: The stimulation of glycolysis by hypoxia in activated monocytes is mediated by AMP-activated protein kinase and inducible 6-phosphofructo-2-kinase. *J Biol Chem* 277:30778–30783, 2002
17. Kessler R, Eschrich K: Splice isoforms of ubiquitous 6-phosphofructo-2-kinase/fructose-2,6-bisphosphatase in human brain. *Mol Brain Res* 87:190–195, 2001
18. Bando H, Atsumi T, Nishio T, Niwa H, Mishima S, Shimizu C, Yoshioka N, Bucala R, Koike T: Phosphorylation of the 6-phosphofructo-2-kinase/fructose 2,6-bisphosphatase/PFKFB3 family of glycolytic regulators in human cancer. *Clin Cancer Res* 11:5784–5792, 2005
19. Watanabe F, Sakai A, Furuya E: Novel isoforms of rat brain fructose 6-phosphate 2-kinase/fructose 2,6-bisphosphatase are generated by tissue-specific alternative splicing. *J Neurochem* 69:1–9, 1997
20. Watanabe F, Furuya E: Tissue-specific alternative splicing of rat brain fructose 6-phosphate 2-kinase/fructose 2,6-bisphosphatase. *FEBS Lett* 458:304–308, 1999
21. Lehmann JM, Moore LB, Smith-Oliver TA, Wilkison WO, Willson TM, Kliewer SA: An antidiabetic thiazolidinedione is a high affinity ligand for peroxisome proliferator-activated receptor gamma (PPAR gamma). *J Biol Chem* 270:12953–12956, 1995
22. Okuno A, Tamemoto H, Tobe K, Ueki K, Mori Y, Iwamoto K, Umesono K, Akanuma Y, Fujiwara T, Horikoshi H, Yazaki Y, Kadowaki T: Troglitazone increases the number of small adipocytes without the change of white adipose tissue mass in obese Zucker rats. *J Clin Invest* 101:1354–1361, 1998
23. Reed BC, Lane MD: Insulin receptor synthesis and turnover in differentiating 3T3-L1 preadipocytes. *Proc Natl Acad Sci U S A* 77:285–289, 1980
24. Reed BC, Kaufmann SH, Mackall JC, Student AK, Lane MD: Alterations in insulin binding accompanying differentiation of 3T3-L1 preadipocytes. *Proc Natl Acad Sci U S A* 74:4876–4880, 1977
25. Chen H, Charlat O, Tartaglia LA, Woolf EA, Weng X, Ellis SJ, Lakey ND, Culpepper J, Moore KJ, Breitbart RE, Duyk GM, Tepper RI, Morgenstern JP: Evidence that the diabetes gene encodes the leptin receptor: identification of a mutation in the leptin receptor gene in db/db mice. *Cell* 84:491–495, 1996
26. Kahn CR, White MF, Shoelson SE, Backer JM, Araki E, Cheatham B, Csermely P, Folli F, Goldstein BJ, Huertas P, et al.: The insulin receptor and its substrate: molecular determinants of early events in insulin action. *Recent Prog Horm Res* 48:291–339, 1993
27. Sun XJ, Rothenberg P, Kahn CR, Backer JM, Araki E, Wilden PA, Cahill DA, Goldstein BJ, White MF: Structure of the insulin receptor substrate IRS-1 defines a unique signal transduction protein. *Nature* 352:73–77, 1991
28. Lavan BE, Lane WS, Lienhard GE: The 60-kDa phosphotyrosine protein in insulin-treated adipocytes is a new member of the insulin receptor substrate family. *J Biol Chem* 272:11439–11443, 1997
29. Virkamaki A, Ueki K, Kahn CR: Protein-protein interaction in insulin signaling and the molecular mechanisms of insulin resistance. *J Clin Invest* 103:931–943, 1999
30. Lang CH, Bagby GJ, Spitzer JJ: Glucose kinetics and body temperature after lethal and nonlethal doses of endotoxin. *Am J Physiol* 248:R471–R478, 1985
31. Orlinska U, Newton RC: Role of glucose in interleukin-1 beta production by lipopolysaccharide-activated human monocytes. *J Cell Physiol* 157:201–208, 1993
32. Guida E, Stewart A: Influence of hypoxia and glucose deprivation on tumour necrosis factor-alpha and granulocyte-macrophage colony-stimulating factor expression in human cultured monocytes. *Cell Physiol Biochem* 8:75–88, 1998
33. Deprez J, Vertommen D, Alessi DR, Hue L, Rider MH: Phosphorylation and activation of heart 6-phosphofructo-2-kinase by protein kinase B and other protein kinases of the insulin signaling cascades. *J Biol Chem* 272:17269–17275, 1997
34. Rider MH, Bertrand L, Vertommen D, Michels PA, Rousseau GG, Hue L: 6-phosphofructo-2-kinase/fructose-2,6-bisphosphatase: head-to-head with a bifunctional enzyme that controls glycolysis. *Biochem J* 381:561–579, 2004
35. Myers MG Jr, Backer JM, Sun XJ, Shoelson S, Hu P, Schlessinger J, Yoakim M, Schaffhausen B, White MF: IRS-1 activates phosphatidylinositol 3′-kinase by associating with src homology 2 domains of p85. *Proc Natl Acad Sci U S A* 89:10350–10354, 1992
36. Sobrino F, Gualberto A: Hormonal regulation of fructose 2,6-bisphosphate levels in epididymal adipose tissue of rat. *FEBS Lett* 182:327–330, 1985
37. Navarro-Sabate A, Manzano A, Riera L, Rosa JL, Ventura F, Bartrons R: The human ubiquitous 6-phosphofructo-2-kinase/fructose-2,6-bisphosphatase gene (PFKFB3): promoter characterization and genomic structure. *Gene* 264:131–138, 2001
38. Marsin AS, Bertrand L, Rider MH, Deprez J, Beauloye C, Vincent MF, Van den Berghe G, Carling D, Hue L: Phosphorylation and activation of heart PFK-2 by AMPK has a role in the stimulation of glycolysis during ischaemia. *Curr Biol* 10:1247–1255, 2000

39. Lefebvre V, Mechin MC, Loucks MP, Rider MH, Hue L: Signaling pathway involved in the activation of heart 6-phosphofructo-2-kinase by insulin. *J Biol Chem* 271:22289–22292, 1996
40. Bertrand L, Alessi DR, Deprez J, Deak M, Vincent E, Rider MH, Hue L: Heart 6-phosphofructo-2-kinase activation by insulin results from Ser-466 and Ser-483 phosphorylation and requires 3-phosphoinositide-dependent kinase-1, but not protein kinase B. *J Biol Chem* 274:30927–30933, 1999
41. Manes NP, El-Maghrabi MR: The kinase activity of human brain 6-phosphofructo-2-kinase/fructose-2,6-bisphosphatase is regulated via inhibition by phosphoenolpyruvate. *Arch Biochem Biophys* 438:125–136, 2005
42. Rider MH, Hue L: Regulation of fructose 2,6-bisphosphate concentration in white adipose tissue. *Biochem J* 225:421–428, 1985

International Immunology Advance Access published October 12, 2005

International Immunology 2005; 1 of 10
doi:10.1093/intimm/dxh330

Antigenic structures recognized by anti-β2-glycoprotein I auto-antibodies

Hideki Kasahara[1], Eiji Matsuura[2], Keiko Kaihara[2], Daisuke Yamamoto[3], Kazuko Kobayashi[2], Junko Inagaki[2], Kenji Ichikawa[1], Akito Tsutsumi[1], Shinsuke Yasuda[1], Tatsuya Atsumi[1], Tatsuji Yasuda[2] and **Takao Koike[1]**

[1]Department of Medicine II, Hokkaido University Graduate School of Medicine, Sapporo 060-8638, Japan
[2]Department of Cell Chemistry, Okayama University Graduate School of Medicine and Dentistry, Okayama 700-8558, Japan
[3]Biomedical Computation Center, Osaka Medical College, Takatsuki 569-8686, Japan

Keywords: anti-phospholipid antibody, anti-phospholipid syndrome, B cell epitope

Abstract

β2-Glycoprotein I (β2-GPI) is a major antigen for anti-cardiolipin antibodies and their epitopes are cryptic. Conformation of each domain of β2-GPI was optimized from its crystal structure by energy minimization and by molecular dynamics simulation. Three electrostatic interactions, i.e. D^{193}–K^{246}, D^{222}–K^{317} and E^{228}–K^{308}, were observed between domains IV and V in the optimized structure that was constructed based on the consensus sequences obtained by the phage-displayed random peptide library. Antigenic structures determined by the epitope mapping mainly consisted of hydrophobic amino acids located on two discontinuous sequences in domain IV. These amino acid clusters, as an epitope, were covered by domain V and were of a hidden nature. A similar but incomplete counterpart to the epitopic clusters was found in domain I but was not in domains II or III. Binding of anti-β2-GPI auto-antibodies to solid-phase β2-GPI was significantly reduced either by L replacement for W^{235}, a common amino acid component for the epitopes, or by V replacement for all of D^{193}, D^{222} and E^{228}. Structural analysis indicated a hypothesis that these electrostatic interactions between domains IV and V retained exposure to W^{235} and that epitope spreading occurred in the region surrounding W^{235}. Thus, epitopic structures recognized by anti-β2-GPI auto-antibodies are cryptic and inter-domain electrostatic interactions are involved in their in exposure.

Introduction

The anti-phospholipid syndrome (APS) is a multi-system disorder characterized by arterial/venous thrombosis and pregnancy complication (1–4). Anti-phospholipid antibodies, in particular, anti-cardiolipin antibodies (aCLs) and lupus anticoagulant (5), are of considerable clinical importance in APS. In 1990, three individual research groups reported that a 50 kD plasma co-factor is required for the binding of such aCL to cardiolipin (CL) (6–8)and β2-glycoprotein I (β2-GPI), which binds to anionic phospholipids (PLs), is currently thought to be the major antigen for aCL in APS patients.

We reported that aCL-recognized cryptic epitopes appear on the β2-GPI molecule only when β2-GPI interacts with lipid membranes containing anionic PLs, such as CL, or also with a polyoxygenated polystyrene surface (9, 10). We also reported that domain IV of β2-GPI was dominantly involved in expression of antigenicity for anti-β2-GPI auto-antibodies (11). Other research groups reported the presence of anti-β2-GPI auto-antibodies directed to domain V (12, 13) or to domain I (13). It has also been proposed that binding of β2-GPI to anionic PLs increased the local concentration of β2-GPI, thus leading to an increase in intrinsic affinity and binding of the antibody to β2-GPI, an event which argues against the interpretation that epitopes for aCL are cryptic (14, 15).

β2-GPI, a 50-kD protein with a carbohydrate content of 17%, is present in normal human plasma at ~200 μg ml^{-1} and was apparently first described by Schultze *et al.* (16). β2-GPI is composed of five homologous motifs of ~60 amino acids which contain highly conserved half-cysteine residues related to the formation of two internal disulfide bridges. These repeating motifs were designated as short consensus repeats (SCR)/complement control protein (CCP) repeats or sushi domains (17–19). The fifth domain is a modified form that contains 82 amino acid residues and 6 half cysteines. The primary amino acid sequence is highly conserved (>80%) among human, bovine and mouse counterparts (20). The crystal structure of human β2-GPI was recently reported (21, 22).

Correspondence to: T. Koike; E-mail: tkoike@med.hokudai.ac.jp

Transmitting editor: S. Izui

Received 27 September 2004, *accepted* 6 September 2005

2 *Epitopes recognized by anti-phospholipid antibodies*

We characterized epitopic structures for anti-β2-GPI autoantibodies derived from APS by making use of epitope mapping based on the crystal structure of β2-GPI. Our results show that cryptic epitopes for monoclonal anti-β2-GPI autoantibodies located on a particular region in its domain IV and that the region is naturally hidden by domain V. Three electrostatic interactions between domains IV and V were involved in both crypt and exposure of the amino acid clusters, as an epitope.

Methods

Microtiter plates

Plain plates (Sumilon S-type) and polyoxygenated plates (Sumilon C-type) were obtained from Sumitomo Bakelite Co., Ltd (Tokyo, Japan). Densities of oxygen atoms covalently introduced onto the polystyrene surfaces were analyzed by X-ray photoelectron spectroscopy and the results were as follows: plain plate, C–O (1.3 mol%); polyoxygenated plate, C–O (10.5 mol%); C=O (5.6 mol%); O–C=O (3.7 mol%).

Sera and mAbs

Anti-β2-GPI antibody-positive sera were obtained from systemic lupus erythematosus patients who fulfilled the criteria of the American Rheumatism Association revised in 1982. All patients had significantly high levels of β2-GPI-dependent aCL, as compared with healthy subjects, and had one or more symptoms of APS, i.e. thromboembolic complications (venous and/or arterial), recurrent spontaneous abortion and/or thrombocytopenia. Monoclonal anti-β2-GPI auto-antibodies, EY1C8, EY2C9 and TM1G2, were derived from the APS patients (23). Patients EY and TM had recurrent fetal losses and recurrent deep vein thrombosis accompanied by multiple pulmonary embolism, respectively. EY1C8 and EY2C9 competitively inhibit 50–80% of the IgG aCL activity of sera from the patient from whom these monoclonal aCLs were established. A mouse monoclonal anti-β2-GPI auto-antibody, WB-CAL-1, was established from splenocytes of a (NZW × BXSB) F1 male mouse (24). Pathogenic roles of these mAbs have been known *in vitro* and *in vivo*. Five mouse monoclonal anti-human β2-GPI antibodies, Cof-18, Cof-20, Cof-21, Cof-22 and Cof-23, were established from the splenocytes of BALB/c mice immunized with human β2-GPI in CFA (11, 25).

Biopanning and selection of clones from random peptide libraries

Consensus peptide sequences recognized by anti-β2-GPI antibodies were obtained with combinatorial libraries of a 7-mer and/or 12-mer random peptide fused to a minor coat protein (pIII) of the filamentous coilphage, M13 (PH.D-7 and/or PH.D-12 Phage Display Peptide Library Kit, New England Biolabs Inc., Beverly, MA, USA). These libraries consist theoretically of 2.0×10^9 or 1.9×10^9 electroporated sequences, respectively. A plain plate was coated by incubating with 150 μl of anti-β2-GPI mAbs (100 μg ml^{-1}) in 0.1 M $NaHCO_3$ overnight at 4°C, followed by blocking with 10 mM Tris–HCl, 150 mM NaCl, pH 7.4 [Tris-buffered saline (TBS)] containing 5 mg ml^{-1} of BSA for 1 h. The plate was washed six times with 200 μl of TBS containing 0.05% Tween 20 (TBS–Tween) and 100 μl of phages (2×10^{12} ml^{-1} in TBS–Tween), then incubated for 1 h. Following 10 washings with TBS–Tween, bound phages were eluted with 0.2 M glycine–HCl (pH 2.2) containing 1 mg ml^{-1} of BSA. After three rounds of selection and amplification with the mAbs, the clones were isolated and sequenced.

Optimization of the structure of human β2-GPI

A conformation of each domain was first constructed from the crystal structure (implemented in Protein Data Bank: 1C1Z) and was then optimized by 2000 cycles of energy minimization by the CHARMm program (26), with hydrophilic hydrogen atoms and TIP3 water molecules (27). Molecular dynamics simulation (5 ps) was then done with a 0.002 ps time step. Cutoff distance for non-bonded interactions was set to 15+ and the dielectric constant was 1.0. A non-bonded pair list was updated every 10 steps. The most stable structure of each domain in the dynamics iterations was then optimized by 2000 cycles of energy minimization. The final structures of domains I, II, III, VI and V consisted of 1867, 1722, 2097, 1828 and 2602 atoms, including 443, 408, 515, 435 and 598 TIP3 water molecules, respectively.

A structure of complex domains IV and V was further constructed by considering the location of the oligosaccharide attachment site in domain IV, location of epitopic regions of the Cof-18 and Cof-20 mAbs, junction between domains IV and V and the molecular surface charges of both domains. This model was again optimized by molecular dynamics simulation and by energy minimization. The final structure consisting of 3775 atoms, including hydrophilic hydrogen atoms and 807 TIP3 water molecules had a total energy of -2.43×10^4 kcal mol^{-1} with a root mean square (r.m.s.) force of 0.985 kcal mol^{-1}. A model of mutant domain IV in which D^{193}, D^{222} and E^{228} were replaced by valines (V) or of cleaved domain V at a K^{317}–T^{318} was constructed. After optimization, the final structures consisted of 3774 and 3839 atoms, including hydrophilic hydrogen atoms and 808 and 827 TIP3 water molecules and had a total energy of -2.42×10^4 and -2.02×10^4 kcal mol^{-1} with a r.m.s. force of 0.892 and 0.979 kcal mol^{-1}, respectively.

Production of β2-GPI mutant proteins

By site-directed mutagenesis, we designed four kinds of β2-GPI mutant proteins of which three particular amino acids, i.e. D^{193}, D^{222} and/or E^{228} were replaced by V. Another mutant, W^{235} replaced by L, was also designed. The isolation and sequencing of a full-length cDNA for human β2-GPI was as described (20). The cDNA was digested with *Eco*R1 and *Bgl*II and ligated to the corresponding site of the pVL1393 transfer vector. To assess the mutation, we used the GeneEditor *in vitro* site-directed mutagenesis system (Promega Corp., Madison, WI, USA) and the sequence of primers used is as follows: 5′-TGCCCATTCCCATCAAGACCAGTCAATG-3′ for a mutant $D^{193} \rightarrow V$ (GAC → GTC), 5′-GGATATTCTCTGGTTGGCCCG-GAAGAAATAG-3′ for a mutant $D^{222} \rightarrow V$ (GAT → GTT), 5′-GGCCCGGAAGAAATAGTATGTACCAAACTG-3′ for a mutant $E^{228} \rightarrow V$ (GAA → GTA), 5′-TGCCCATTCCCATCAAGACCA-GTCAATG-3′ and 5′-CTCTGGTTGGCCCGGAAGAAATAGTA-TGTACC-3′ for a mutant 'triple', $D^{193} \rightarrow V$ (GAC → GTC),

D^{222} → V (GAT → GTT) and E^{228} → V (GAA → GTA) and 5′-TGTACCAAACTGGGAAACTTGTCTGCCATGCC-3′ for a mutant W^{235} → L (TGG → TTG). A DNA sequence of the mutants was verified by analysis using Prism Model 310 (PE Applied Biosystems, Foster City, CA, USA). Recombinant β2-GPI and its mutant proteins were produced in the baculovirus *Spodoptera frugiperda* (Sf-9) expression system (11) using linearized virus cDNA (Baculogold, Pharmingen, San Diego, CA, USA). β2-GPI proteins were purified from serum-free culture media (Sf-900 II, Life Technologies, Grand Island, NY, USA) using anti-β2-GPI mAb affinity column chromatography. Apparent molecular mass of these mutant proteins in SDS-PAGE was 43 kD and there were no significant changes (data not shown).

ELISA for anti-β2-GPI antibodies

Anti-β2-GPI ELISA was done as described (9) but with slight modification. A polyoxygenated plate was coated by incubation with 50 μl per well of recombinant β2-GPI or its mutant proteins, dissolved at a concentration of 2.5 μg ml^{-1} in PBS, pH 7.4, overnight at 4°C. The plates were blocked with 200 μl of PBS containing 3% gelatin (Difco Laboratories, MI, USA) in PBS. Human or mouse anti-β2-GPI mAbs diluted with PBS containing 0.5% gelatin were applied for 1 h. Antibody binding to β2-GPI was probed by HRP-conjugated anti-mouse IgG or anti-human IgG/IgM and *o*-phenylenediamine solution (0.2 mg ml^{-1}) containing 0.01% H_2O_2 was applied for 10 min. Color reaction was halted by adding 100 μl of 2 N H_2SO_4 and optical density was measured at 492 nm. Between each step, we used 200 μl of PBS containing 0.05% Tween 20 (PBS–Tween) for extensive washings.

Inhibition ELISA for the binding between β2-GPI and anti-β2-GPI mAb

β2-GPI at the concentration of 10 μg ml^{-1} was coated on the polyoxygenated plates and was blocked in the same way as described above. Solutions of WB-CAL-1 (1 μg ml^{-1}) together with different concentrations (up to 1 μM) of β2-GPI or triple mutant of β2-GPI, in the presence or absence of CL–liposome (10 μg ml^{-1}), were distributed to the wells in triplicate. HRP-conjugated anti-mouse mAb was utilized for detection.

Results

Epitopic structures of anti-β2-GPI antibodies

Peptide libraries displayed on filamentous phages were used to define the antigenic structure specific for anti-β2-GPI mAbs. In all screenings, we carried out at least three rounds of biopanning with coated antibodies on a plain plate. After the latest biopanning, 20- to 10,000-fold increase in the number of eluted phages and 6 to 10 clones were randomly picked up and nucleotide sequences coding fused peptides were analyzed (Table 1). The conformation of each domain of β2-GPI was constructed from the crystal structure's coordinates of human β2-GPI implemented in the Brookhaven Protein Data Bank as 1C1Z. We had earlier characterized the fine specificities of Cof-18, Cof-20 and Cof-21 mAbs, established from human β2-GPI immunized BALB/c mice (11). All these antibodies recognize the native structure of human β2-GPI and their epitopes are located on the surface of domains V, III and IV of β2-GPI in solution, respectively. As shown in Fig. 1, all antigenic structures for these mAbs were identified on the outer surface in individual domains. Antigenic structures for human anti-β2-GPI auto-mAbs, namely EY1C8, EY2C9 and TM1G2, and for a mouse monoclonal auto-antibody, WB-CAL-1, were identified in domain IV (Fig. 2). In case of EY1C8, two possible candidates for the antigenic structure have to be considered (Table 2, Fig. 2). All these epitopes were located on two individual loops, i.e. the N- and C-terminal loops of the domain.

Structural model of the domain IV–V complex

To investigate interactions between domains IV and V, a structural model of the domain IV–V complex of β2-GPI in solution was constructed by considering crypticity of the epitope for the monoclonal auto-antibodies (i.e. EY1C8, EY2C9, TM1G2 and WB-CAL-1) and exposing of epitopic structures for Cof-18 and Cof-21. The r.m.s. deviation of the main-chain structure of each domain in the complex model and the original X-ray structure was <1.52 Å with superimpositions of only each domain, and the secondary structure of the model was not significantly altered by optimization. Three electrostatic interactions (D^{193}–K^{246}/K^{250}, D^{222}–K^{305} and E^{228}–K^{308}) between domains IV and V, and the interaction of K^{242}–E^{302} in the IV–V junction were the only significant differences observed (Fig. 3). The model was more stable than the unbent structure shown in the X-ray structure. Although W^{235}, exposed in the X-ray structure, was naturally covered by domain V in the model, N^{234}, an oligosaccharide attachment site, was exposed in both structures. All the above antigenic structures for EY1C8, EY2C9, TM1G2 and WB-CAL-1 on domain IV were partly hidden by the overlying of domain V.

Alteration on antigenicity for anti-β2-GPI antibodies by the mutations

Binding of anti-β2-GPI mAbs to the solid-phase β2-GPI mutant proteins was then determined (Fig. 4). Binding of the mouse

Table 1. Sequences of synthetic oligonucleotides used for mutagenesis

Mutant	Synthetic primer	Codon change
D^{193} → V	5′-TGCCCATTCCCATCAAGACCAGTCAATG-3′	GAC → GTC
D^{222} → V	5′-GGATATTCTCTGGTTGGCCCGGAAGAAATAG-3′	GAT → GTT
E^{228} → V	5′-GGCCCGGAAGAAATAGTATGTACCAAACTG-3′	GAA → GTA
Triple (D^{193} → V, D^{222} → V, E^{228} → V)	5′-TGCCCATTCCCATCAAGACCAGTCAATG-3′ 5′-CTCTGGTTGGCCCGGAAGAAATAGTATGTACC-3′	GAC → GTC GAT → GTT, GAA → GTA
W^{235} → L	5′-TGTACCAAACTGGGAAACTTGTCTGCCATGCC-3′	TGG → TTG

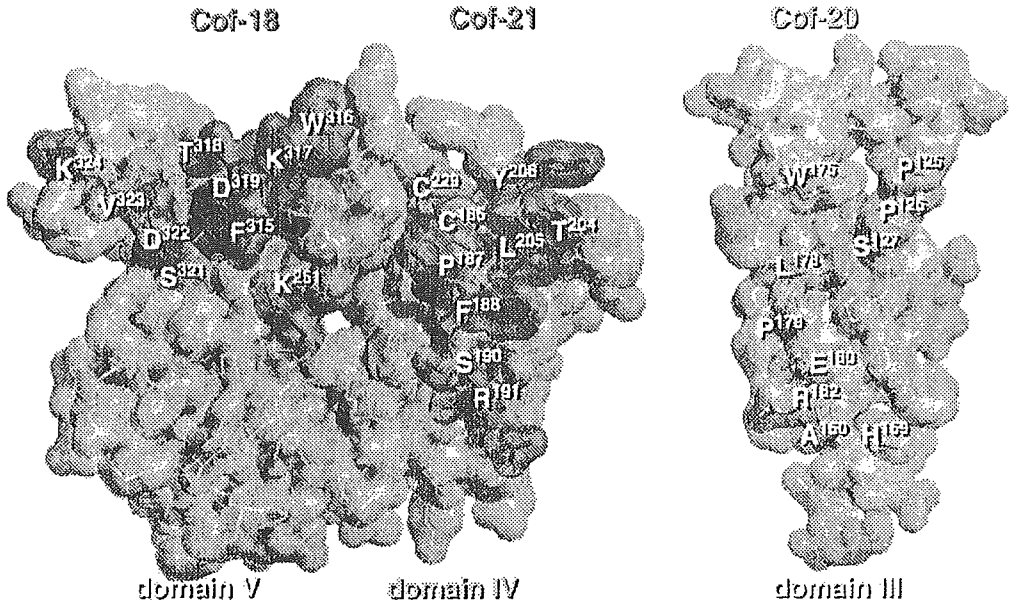

Fig. 1. Epitopic structures recognized by mouse anti-β2-GPI mAbs, Cof-18, Cof-20 and Cof-21. All antigenic regions for Cof-18, Cof-21 and Cof-20 were present on the outer surface of domains V, IV and III, respectively. Each amino acid residue composed of these epitopes is displayed by a bold stick and space-filling model with a residue number and the others by a light stick and space-filling model. The correspondences of the deduced amino acid sequences from the phage-displayed peptide libraries and epitopic regions on the β2-GPI molecule are summarized in Table 2.

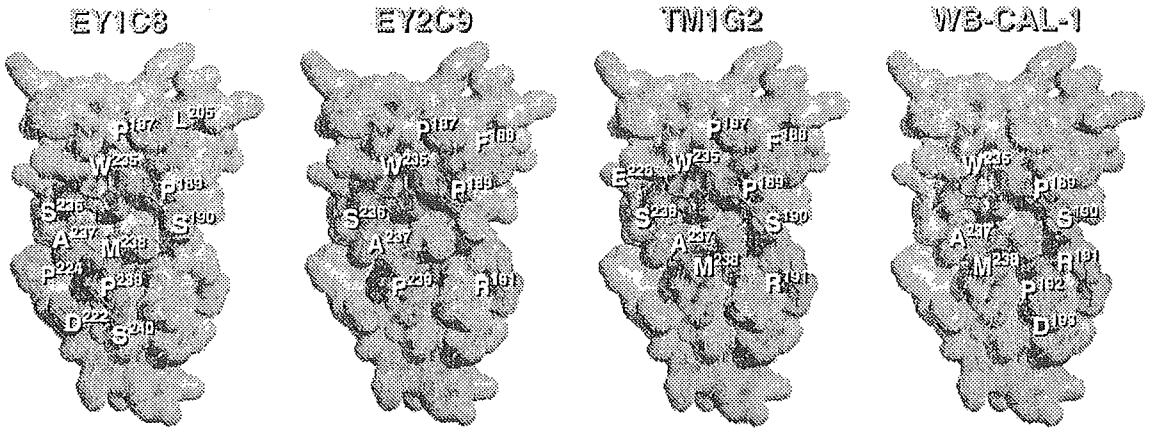

Fig. 2. Antigenic regions for auto-antibodies, i.e. EY1C8, EY2C9, TM1G2 and WB-CAL-1 mAbs were present in domain IV. Each amino acid residue composed of these epitopes is colored violet with a residue number and the others by green. Correspondences of the deduced amino acid sequences from the phage-displayed peptide libraries and epitopic regions on the β2-GPI molecule are summarized in Table 1.

anti-human β2-GPI mAbs Cof-21 which recognize a native structure in domain IV (Fig. 1) was not affected by any V replacements for D^{193}, D^{222} and E^{228}. In contrast, binding of human and mouse anti-β2-GPI auto-mAbs, i.e. EY2C9 and WB-CAL-1 (recognized a cryptic epitope in domain IV), was affected considerably by all four types of mutations, and almost completely disappeared by the triple one. It was supported by our model that the reduction of antigenicity might be caused by turning of W^{235}, which might have the major role for epitopic construction, into the inner side of domain IV, due to the interaction with domain V via these three hydrogen bonds. The side chain of the W residue appeared outside of the VI–V model. In contrast, the side chain directed to the inner space of the IV domain was displayed in the X-ray structure and in our other model with the triple mutation (Fig. 5).

When we tested for 30 anti-β2-GPI antibody-positive APS serum samples, antibody binding in 24 serum samples (80%) was significantly attenuated by the triple mutation (Fig. 6A). The 'type A' group was defined as having higher binding to native β2-GPI compared with the mutant. In contrast, six samples (20%) showed increased binding to the mutant

Table 2. Consensus amino acid sequences deduced from phage libraries and epitopes for anti-β2-GPI antibodies

Antibody (location of epitope)	Phage no.	Consensus sequences from phage libraries	Frequency	Corresponding amino acid residues on the β2-GPI molecule
Cof-18 (domain V)	Cof-18-1	GMKLTSEQKAML	4/9	$*\ *K^{324}V^{325}*S^{321}D^{322}*K^{251}**P^{315}D^{319}T^{316}W^{316}*S^{317}$
	Cof-18-2	SDWRLMFESWIR	3/9	
Cof-20 (domain III)	Cof-20	AHKDHVVSTWVP	5/10	$A^{160}H^{159}R^{182}E^{180}*\ P^{179}\ L^{176}S^{127}*\ W^{175}P^{126}P^{125}$
Cof-21 (domain IV)	Cof-21	NFCASCLLPVSR	7/10	$*Y^{206}C^{229}L^{205}T^{204}C^{166}**P^{167}F^{166}\ S^{190}\ R^{191}$
EY1C8 (domain IV)	EY1C8-1	DLFVTAW	4/9	$^{a}D^{222}S^{240}P\ ^{239}M^{238}*S^{190}P^{169}W^{235}P^{167}L^{205}***$
	EY1C8-2	SLMVSPWPLHGV	4/9	$^{a}D^{222}S^{240}P\ ^{239}M^{238}A^{237}S^{236}*W^{235}P^{167}L^{205}***$
EY2C9 (domain IV)	EY2C9	HNIWSAPRLIFN	4/10	$**P^{167}W^{235}S^{236}A^{237}P^{239}R^{191}\ *\ P^{169}F^{166}\ *$
TM1G2 (domain IV)	TM1G2-1	DLTIMPWSLYPP	4/10	$E^{226}*S^{236}A^{237}M^{238}*W^{235}*P^{167}S^{190}F^{166}P^{169}R^{191}$
	TM1G2-2	TMMQTMSFLRGF	2/10	
WB-CAL-1 (domain IV)	WB-CAL-1	SLWQDRLNAMQS	5/6	$S^{190}I^{169}W^{235}*D^{193}R^{191}P^{192}*A^{237}M^{238}**$

[a]Two possible correspondences are considered with EY1C8 libraries.

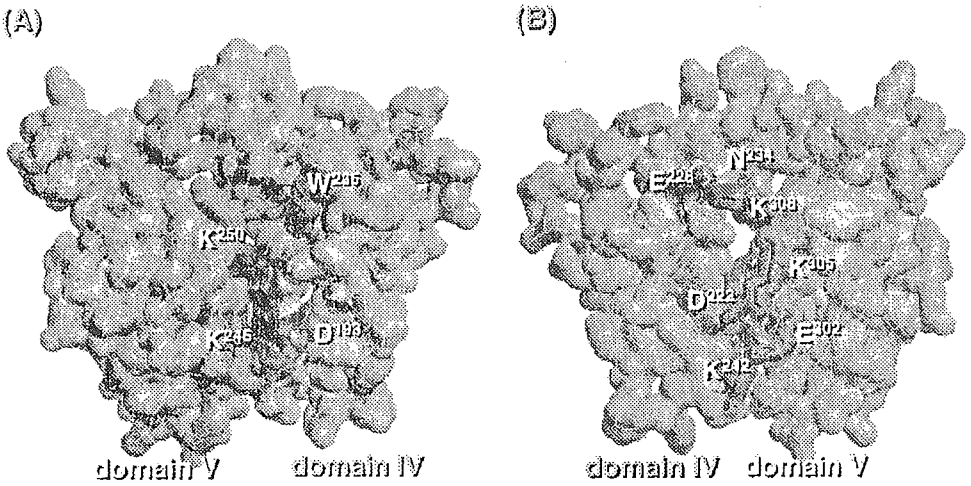

Fig. 3. Interaction of domains IV and V. (A) A space-filling model of domains IV–V is shown from one direction (left) and from another one (right) and the structure of each domain is displayed in different colors: domain IV, blue; domain V, yellow.

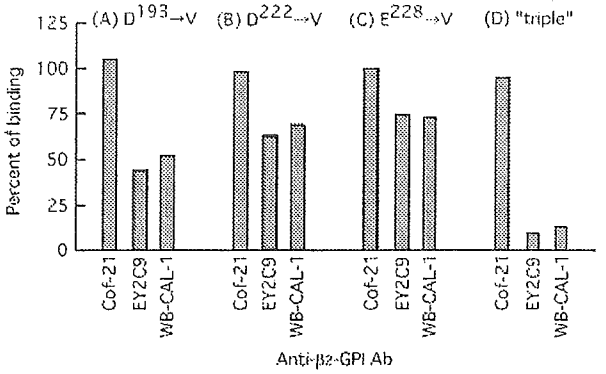

Fig. 4. Binding of anti-β2-GPI mAbs to solid-phase mutant proteins. Antibody binding to the mutant proteins is indicated (as a percent of control) and as compared with that to control β2-GPI. mAbs (1 μg ml^{-1}) were used for the assay.

protein (defined as 'type B'). Two typical binding profiles of anti-β2-GPI antibodies in sera of patients with APS are shown in Fig. 6(B). The above-described major antibodies showed a binding profile similar to that of the type A antibody and a significantly reduced binding to the triple mutant protein was likely the result of the sum of weak reductions caused by each mutation for D^{193}, D^{222} or E^{228}. In contrast, the latter minor group of antibodies revealed a profile similar to that of the type B antibody.

The importance of the domain IV–V interaction was also investigated using an inhibition assay. Binding between WB-CAL-1 and β2-GPI coated on polyoxygenated plates was disrupted by the addition of β2-GPI in the presence of CL–liposome in a dose-dependent manner. This inhibition was not observed by the addition of β2-GPI alone or the triple mutant of β2-GPI with the CL–liposome (Fig. 7). In the absence of the CL–liposome, neither native β2-GPI nor the triple mutant had any inhibition for the binding of WB-CAL-1.

As shown in Table 1 and Fig. 3, amino acid W^{235} was always used to form the antigenic structures recognized by anti-β2-GPI auto-antibodies so that we prepared another mutant protein in which W^{235} was replaced by L. With this replacement, β2-GPI binding of auto-antibodies, i.e. EY2C9, WB-CAL-1, and of antibodies in 30 of the anti-β2-GPI antibody-positive APS serum samples was significantly diminished (Fig. 8). In contrast, the mutation did not affect antibody binding of mouse anti-human β2-GPI mAb Cof-21 (Fig. 8A).